Lattice Boltzmann scheme for mixture modeling: analysis of the continuum diffusion regimes recovering Maxwell–Stefan model and incompressible Navier–Stokes equations

Pietro Asinari

Department of Energetics, Politecnico di Torino,

Corso Duca degli Abruzzi 24, Torino, Italy

(Dated: September 25, 2009)

Abstract

A finite difference Lattice Boltzmann scheme for homogeneous mixture modeling, which recovers Maxwell–Stefan diffusion model in the continuum limit, without the restriction of the mixture-averaged diffusion approximation, was recently proposed [P. Asinari, PRE, Vol. 77, 056706, 2008]. The theoretical basis is the BGK-type (Bhatnagar-Gross-Krook-type) kinetic model for gas mixtures [P. Andries, K. Aoki and B. Perthame, JSP, Vol. 106, N. 5/6, 2002]. In the present paper, the recovered macroscopic equations in the continuum limit are systematically investigated by varying the ratio between the characteristic diffusion speed and the characteristic barycentric speed. It comes out that the diffusion speed must be at least one order of magnitude (in terms of Knudsen number) smaller than the barycentric speed, in order to recover the correct Navier-Stokes equations for mixtures in the incompressible limit. Moreover some numerical tests are reported. In particular, (1) the solvent and dilute test cases are considered, because they are limiting cases in which the Maxwell–Stefan model reduces automatically to Fickian cases. Moreover, some tests based on the (2) Stefan diffusion tube are reported for proving the complete capabilities of the proposed scheme in solving Maxwell–Stefan diffusion problems. The proposed scheme agrees well with the expected theoretical results.

PACS numbers: 47.11.-j, 05.20.Dd

I. INTRODUCTION

Recently, the lattice Boltzmann method (LBM) has been proposed as simple alternative to solve simplified kinetic models. Starting from some pioneer works [1–3], the method has reached a more systematic fashion [4, 5] by means of a better understanding of the connections with the continuous kinetic theory [6, 7]. A more complete overview of LBM can be found in some review papers [8, 9] and some books [10–12].

In the present paper, the attention will be focused on the development of an LBM scheme for *mass diffusion modeling* in the continuum limit. For this goal, the so-called *single-operator approach* [13, 14] was proposed. Essentially, the averaged effect due to both self-collisions and cross-collisions is described by means of a global BGK-like collisional operator. In order to properly take into account the momentum exchange among the mixture components, some popular lattice Boltzmann models for mixtures are based on pseudo-potential interactions [15–17] or heuristic free energies [18–21].

On the other hand, some models based on the *multiple-operator approach* have been proposed: each species relaxes towards its equilibrium configuration according to its specific relaxation frequency and some coupling must be considered in order to describe the momentum exchange. Some models [22, 23] adopt a *force coupling* in the momentum equations, which derives from a linearized kinetic term, while other models [24–26] avoid any linearization of the coupling effect by *two collisional operators* (the first for self collisions and the second for cross collisions).

Finally [27], another LBM scheme, has been proposed by means of a variational procedure aiming to minimize a proper H function defined on the discrete lattice. In particular, the new proposed scheme [27], when more than two components are considered, recovers the macroscopic equations of the Maxwell–Stefan model, which properly takes into account non-ideal effects (osmotic diffusion, reverse diffusion and diffusion barrier), neglected by simpler Fick model. The proposed model consistently recovers the Maxwell–Stefan diffusion equations in the continuum limit only within the macroscopic mixture-averaged diffusion approximation (MADA) [30], i.e. only if proper mixture-averaged diffusion coefficients for each component are considered.

In the present paper, a further step is taken in comparing the model proposed by the same author [33] and that described in Ref. [27]. Actually the mixture averaged diffusion

2

approximation (MADA) is substantially based on modest deviations of the single species flows from the barycentric flow, i.e. on small diffusion velocities with regards to barycentric flow velocities. Hence using MADA is equivalent to assume an upper bound threshold for the ratio between diffusion to barycentric speed. In the present paper, the effects of this ratio on the model proposed by the same author is systematically investigated, in terms of recovered macroscopic equations and their consistenty with Navier-Stokes equations.

This paper is organized as follows. In Section II the adopted LBM scheme is described: the BGK-type proposed model [33] is presented first, the macroscopic equations in the continuum limit are recovered, some macroscopic approximations are recalled and, finally, some details for an efficient implementation are discussed. In particular, some attention is paid for enlighting the role of the diffusion speed. Section III reports some numerical results: solvent and dilute tests, as limiting Fickian cases, and the Stefan diffusion tube, for fully appreciating the capabilities of the scheme. Finally, Section IV summarizes the main results of the paper.

II. LATTICE BOLTZMANN MODEL

A. AAP model

In this paper, we focus on the BGK-type model proposed by Andries, Aoki and Perthame [32], which will be referred to in the following as AAP model, in case of isothermal flow, which is enough to highlight the main features. The model shows some interesting theoretical features, in particular in terms of satisfying the Indifferentiability Principle and fully recovering the macroscopic Maxwell–Stefan model equations in the continuum limit. In the present paper, a Lattice Boltzmann (LB) implementation of the AAP model is discussed. For sake of simplicity, the single–relaxation–time (SRT) version of the model, which implies a fixed Schmidt number, is presented and the external forces are omitted, since the main focus of this paper is on the mass diffusion properties. A more advanced version of the LB model with tunable Schmidt number and external forcing can be found in Ref. [33].

The AAP model is based on only one *global* (i.e., taking into account all the component ς) operator for each component σ, namely

$$\frac{\partial f_\sigma}{\partial \hat{t}} + V_i \frac{\partial f_\sigma}{\partial \hat{x}_i} = \mathbb{C}_\sigma \dot{=} \lambda_\sigma \left[f_{\sigma(*)} - f_\sigma \right],$$ (1)

3

where $\hat{x}_i$, $\hat{t}$, and V_i are the space coordinate divided by the mean free path, the time divided by the mean collision time and the discrete molecular velocity divided by the thermal speed respectively (Boltzmann scaling); f_σ is the distribution function for the component σ; (1) $f_{\sigma(*)}$ is the equilibrium distribution function for the component σ; (2) λ_σ is the relaxation frequency, which, according to the previous scaling, is of the order of unit.

A simplified kinetic equation, such as the discrete velocity model of isothermal BGK equation with constant collision frequencies is often employed as the theoretical basis of LBM. Let us consider a set of discrete microscopic velocities. In particular, V_i is a list of i-th components of the velocities in the considered lattice. Let us consider the two dimensional 9 velocity model, which is called D2Q9. In D2Q9 model, the molecular velocity V_i has the following 9 values:

$$V_1 = \begin{bmatrix} 0 & 1 & 0 & \text{-1} & 0 & 1 & \text{-1} & \text{-1} & 1 \end{bmatrix}^T, \qquad (2)$$

$$V_2 = \begin{bmatrix} 0 & 0 & 1 & 0 & \text{-1} & 1 & 1 & \text{-1} & \text{-1} \end{bmatrix}^T. \qquad (3)$$

The components of the molecular velocity V_1 and V_2 are the lists with 9 elements. Consequently $f = f_{\sigma(*)}, f_\sigma$ is a list of discrete distribution functions corresponding to the velocities in the considered lattice. Let f and g be the lists defined by $f = [f_0, f_1, f_2, \cdots, f_8]^T$ and $g = [g_0, g_1, g_2, \cdots, g_8]^T$. Then, hg is the component-wise list defined by $[f_0 g_0, f_1 g_1, f_2 g_2, \cdots, f_8 g_8]^T$. The sum of all the elements of the list h is denoted by $\langle h \rangle$, i.e. $\langle h \rangle = \sum_{\alpha=0}^{8} f_\alpha$.

In the following subsections, the main elements of the scheme, i.e. (1) the definition of the local equilibrium $f_{\sigma(*)}$ and (2) the relaxation frequency λ_σ will be discussed.

1. *Local equilibrium*

In order to define the local equilibrium function $f_{\sigma(*)}$, we need to consider first the hydrodynamic moments. The (dimensionless) density $\hat{\rho}_\sigma$ and momentum $\hat{q}_{\sigma i} = \hat{\rho}_\sigma \hat{u}_{\sigma i}$ are defined by

$$\hat{\rho}_\sigma = \langle f_\sigma \rangle, \qquad \hat{q}_{\sigma i} = \hat{\rho}_\sigma \hat{u}_{\sigma i} = \langle V_i f_\sigma \rangle, \qquad (4)$$

where f_σ is the distribution function for the component σ.

Contrarily to what happens for the single fluid modeling, the previous momentum is not conserved. Hence the key idea of the AAP model is that the local equilibrium is expressed

4

as a function of a special velocity $\hat{u}_{\sigma i}^*$, which depends on *all the single component velocities*, namely

$$\hat{u}_{\sigma i}^* = \hat{u}_{\sigma i} + \sum_\varsigma \frac{m^2}{m_\sigma m_\varsigma} \frac{B_{\sigma\varsigma}}{B_{mm}} \hat{x}_\varsigma (\hat{u}_{\varsigma i} - \hat{u}_{\sigma i}), \tag{5}$$

where ς is a dummy index for indicating any generic component in the mixture (including σ itself), m_σ and m_ς are the molecular weights for the component σ and ς respectively; $\hat{x}_\varsigma = \hat{\rho}_\sigma / \hat{\rho}$ (where $\hat{\rho} = \sum_\sigma \hat{\rho}_\sigma$) is the mass fraction; m is the mixture averaged molecular weight defined as $1/m = \sum_\sigma \hat{x}_\sigma / m_\sigma$ or equivalently $m = \sum_\sigma \hat{y}_\sigma m_\sigma$; $B(x, y)$ is the generic resistance function, while $B_{\sigma\varsigma} = B(m_\sigma, m_\varsigma)$ and $B_{mm} = B(m, m)$ are the so-called Maxwell–Stefan diffusion resistance coefficients; and finally $\hat{u}_{\varsigma i}$ and $\hat{u}_{\sigma i}$ are the i-th component of the macroscopic velocity for the species ς and σ respectively. The latter parameters can be interpreted as a macroscopic consequence of the interaction potential between component σ and ς and they can be computed as proper integrals of the generic Maxwellian interaction potential (*kinetic way*) or in such a way to recover the desired macroscopic transport co-efficients (*fluid–dynamic way*). In particular the generic resistance coefficient is a function of both the interacting component molecular weights and the equilibrium thermodynamic state, which depends on the total mixture properties only. Some further details on how to compute these coefficients can be found in [34].

Introducing the *mass*-averaged mixture velocity, namely

$$\hat{u}_i = \sum_\varsigma \hat{x}_\varsigma \hat{u}_{\varsigma i}, \tag{6}$$

the definition given by Eq. (5) can be recasted as

$$\hat{u}_{\sigma i}^* = \hat{u}_i + \sum_\varsigma \left(\frac{m^2}{m_\sigma m_\varsigma} \frac{B_{\sigma\varsigma}}{B_{mm}} - 1 \right) \hat{x}_\varsigma (\hat{u}_{\varsigma i} - \hat{u}_{\sigma i}). \tag{7}$$

Consequently two properties immediately follow. If $m_\sigma = m$ for any component σ, then (Property 1)

$$\hat{u}_{\sigma i}^* = \hat{u}_i + \sum_\varsigma \left(\frac{m^2}{mm} \frac{B_{mm}}{B_{mm}} - 1 \right) \hat{x}_\sigma \hat{x}_\varsigma (\hat{u}_{\varsigma i} - \hat{u}_{\sigma i}) = \hat{u}_i. \tag{8}$$

Multiplying Eq. (5) by $\hat{x}_\sigma$ and summing over all the component yields (Property 2)

$$\sum_\sigma x_\sigma \hat{u}_{\sigma i}^* = \hat{u}_i + \sum_\sigma \sum_\varsigma \left(\frac{m^2}{m_\sigma m_\varsigma} \frac{B_{\sigma\varsigma}}{B_{mm}} - 1 \right) \hat{x}_\sigma \hat{x}_\varsigma (\hat{u}_{\varsigma i} - \hat{u}_{\sigma i}) = \hat{u}_i. \tag{9}$$

By means of the previous quantities, it is possible to define the local equilibrium for the model, namely $f_{\sigma(*)} = \hat{\rho}_\sigma \, \mathcal{M}(\hat{u}_{\sigma i}^*)$, where

$$\mathcal{M}_\alpha(a_i) = w_\alpha \left\{ s_{\sigma\alpha} + 3 \left(V_{1\alpha}\, a_1 + V_{2\alpha}\, a_2 \right) + \frac{9}{2} \left(V_{1\alpha}\, a_1 + V_{2\alpha}\, a_2 \right)^2 - \frac{3}{2} \left[(a_1)^2 + (a_2)^2 \right] \right\}, \tag{10}$$

where

$$w = [4/9, 1/9, 1/9, 1/9, 1/9, 1/36, 1/36, 1/36, 1/36]^T, \tag{11}$$

while $s_{\sigma 0} = (9 - 5\,\varphi_\sigma)/4$, $s_{\sigma\alpha} = \varphi_\sigma$ for $1 \le \alpha \le 8$ and $\varphi_\sigma = \min_\varsigma (m_\varsigma)/m_\sigma \le 1$ is a tunable parameter for taking into account of different molecular weights m_σ. The parameter φ_σ is designed such that $s_{\sigma\alpha}$ is positive for any α. It is possible to define the single species pressure (in terms of lattice units) as $\hat{p}_\sigma = \hat{\rho}_\sigma \varphi_\sigma / 3$ and consequently the single species internal energy as $\hat{e}_\sigma = \hat{p}_\sigma / \hat{\rho}_\sigma = \varphi_\sigma / 3$. The advantage of this technique is that one can use a single mesh for modeling different species, with different molecular weights, without interpolations [26]. However designing the local equilibrium such that the partial pressure takes into account of different molecular weights is not enough to recover the full isothermal macroscopic equations. In the latter case, the dependence of the higher order moments (e.g. the third order moments) on the molecular weight cannot be neglected. In this more general case, a possible solution consists of using different meshes tailored on different speeds of sound and then to interpolate the numerical results [27, 35]. In this paper, since the main goal is represented by the low Mach number flows, the local equilibrium given by Eq. (10) is enough. The asymptotic equations recovered in the continuum limit depend on the previous local equilibrium. The consistency with the Navier-Stokes macroscopic description will be discussed in Section II B by asymptotic analysis.

Clearly $\hat{\rho}_\sigma$ can also be obtained as the moment of $f_{\sigma(*)}$, but this is not the case for $\hat{q}_{\sigma i}$:

$$\hat{\rho}_\sigma = \langle f_{\sigma(*)} \rangle, \qquad \hat{q}_{\sigma i}^* = \langle V_i f_{\sigma(*)} \rangle \neq \hat{q}_{\sigma i} = \langle V_i f_\sigma \rangle. \tag{12}$$

The previous expressions mean that the equilibrium distribution $f_{\sigma(*)}$ has the same mass, but not the same momentum as the current distribution f_σ for the generic single species. The latter discrepancy is the actual driving force ruling the momentum exchange among the components of the mixture.

Taking into account the definition of the local equilibrium, let us verify the zero of the collisional operator $\mathbb{C}_\sigma$ (the original proof is already reported in [32]). Essentially $\mathbb{C}_\sigma$ depends

on $f_{\sigma(*)} = \hat{\rho}_\sigma \mathcal{M}(\hat{u}^*_{\sigma i})$, where $\hat{u}^*_{\sigma i}$ is given by Eq. (5), which depends on all species velocities $\hat{u}_{\varsigma i}$, which are combinations of the moments of f_ς, namely

$$\mathbb{C}_\sigma \left(\text{all } f_\varsigma \right) = \mathbb{C}_\sigma \left(\hat{\rho}_\sigma \, \mathcal{M} \left(\hat{u}^*_{\sigma i} \left(\text{all } \hat{u}_{\varsigma i} \left(f_\varsigma \right) \right) \right) \right).$$

The zero of the previous collisional operator is a set of distributions f^0_ς such that $\mathbb{C}_\sigma \left(\text{all } f^0_\varsigma \right) = 0$ for all species σ. It is easy to search for this set of distributions as

$$f^0_\varsigma = \hat{\rho}_\varsigma \, \mathcal{M} \left(\hat{u}^0_{\varsigma i} \right), \tag{13}$$

where $\hat{u}^0_{\varsigma i}$ is defined such that $\mathcal{M} \left(\hat{u}^*_{\sigma i} \left(\text{all } \hat{u}^0_{\varsigma i} \right) \right) = \mathcal{M} \left(\hat{u}^0_{\varsigma i} \right)$, or equivalently

$$\hat{u}^*_{\sigma i} \left(\text{all } \hat{u}^0_{\varsigma i} \right) = \hat{u}^0_{\varsigma i},$$

which means that $\hat{u}^0_{\varsigma i}$ must be invariant with regards to the transformation $\hat{u}_{\varsigma i} \to \hat{u}^*_{\varsigma i}$. In general, according to the definition given by Eq. (5), the only invariant situation is given by $\hat{u}^0_{\varsigma i} = \hat{u}_i$ for all species, i.e. zero diffusion velocities: hence $f^0_\varsigma = \hat{\rho}_\varsigma \, \mathcal{M} \left(\hat{u}_i \right)$, which is consistent with the full Boltzmann equations for mixtures.

2. Relaxation frequency and Indifferentiability Principle

Some proper tuning strategy is required in order to recover the desired transport coefficients in the continuum limit. The following relations will be proved in the next Section II B, concerning the asymptotic analysis: they are anticipated here for sake of completeness of the proposed model. In particular, the relaxation frequency is selected equal for all the species, namely

$$\lambda_\sigma = \lambda = \frac{\hat{p} \, B_{mm}}{\hat{\rho}} = \frac{\hat{p} \, B(m, m)}{\hat{\rho}}, \tag{14}$$

where $\hat{p} = \sum_\sigma \hat{p}_\sigma$. Since the previous relaxation frequency is the only one for the present model, the other transport coefficients uniquely follow,

$$\nu = \frac{1}{3 \, \lambda}, \tag{15}$$

$$\xi_\sigma = \frac{(2 - \varphi_\sigma)}{3 \, \lambda}, \tag{16}$$

where ν is the kinematic viscosity and ξ_σ is a parameter related to the numerical second viscosity coefficient for the single species (the latter quantity is different from the actual

second viscosity coefficient because compressible effects are not rigorously recovered by the considered lattice). This clearly implies a fixed Schmidt number, i.e. a fixed ratio between the kinematic viscosity and the mean diffusion coefficient. A more advanced version of the LB model with tunable Schmidt number can be found in Ref. [33].

It is immediate to prove that the Indifferentiability Principle is satisfied. If $m_\sigma = m$ for any component σ, then property (8) yields $\hat{u}^*_{\sigma i} = \hat{u}_i$. Consequently, summing over all the species yields

$$\frac{\partial f}{\partial \hat{t}} + V_i \frac{\partial f}{\partial \hat{x}_i} = \lambda \left[f_{\sigma(e)} - f \right], \tag{17}$$

where $f = \sum_\sigma f_\sigma$ and $f_{\sigma(e)} = \hat{\rho}\,\mathcal{M}\left(\hat{u}_i\right)$. The previous limiting case clearly recovers the usual Bhatnagar-Gross-Krook (BGK) model [37] and this proves that the mixture description recovers the single-fluid description, if the single species particles can not be distinguished.

In the next section, the macroscopic equations in the continuum limit are recovered.

B.   Asymptotic analysis by Grad moment system

In this section the macroscopic equations of the LB model are recovered by means of the asymptotic analysis. Many types of asymptotic analysis for LBM exist (Chapman–Enskog expansion, Hilbert expansion, Grad moment expansion,...). The Chapman–Enskog expansion is still the most popular approach to analyze LBM schemes, even though, concerning mixture modeling, it shows some limits, as discussed in Appendix A and in Ref. [25]. On the other hand, the Hilbert expansion proposed by Ref. [38] and derived by kinetic theory [39] offers some advantages, even though all the macroscopic moments must be expanded. Recovering macroscopic equations solved by LBM schemes somehow shares some features in common with the much more complex problem of recovering macroscopic equations from kinetic models. A complete review of the latter problem is beyond the purposes of the present paper, but detailed discussions can be found in Refs. [39]. In this paper, we use a simpler approach based on (1) some proper scaling, (2) the Grad moment system and (3) recursive substitutions [40]. The latter method is not new and it has some features in common with recently proposed asymptotic methods in kinetic theory [41]. Recently the so–called Order of Magnitude Approach has been proposed in order to derive approximations to the Boltzmann equation from its infinite set of corresponding moment equations. Additional information can be found in Ref. [33].

Essentially we follow the same methodology already reported in [33], but with a substantial difference. In Ref. [33], it is assumed that the diffusion velocities are large, which leads to inconsistencies with regards to Navier-Stokes equations, while in the present derivation a more general assumption is considered.

1. Diffusive scaling

First of all, a proper scaling must be introduced for all the relevant physical quantities. In 1971, Sone extended the linearized theory of Boltzmann equation to the case where the Reynolds number is of the order of unity and the extension is carried out by taking into account the von Karman relation among three important parameters, i.e. that the Mach number is of the same order as the product of Reynolds number and the Knudsen number [39]. At the leading order, this yields to the Navier-Stokes set of equations in the incompressible limit. This result is also relevant for LBM with usual stencils, because the latter are restricted to moderate Mach number flows. Hence in the following analysis, the previous procedure is adopted to the proposed model.

The unit of space coordinate and that of time variable in Eq. (1) are the mean free path l_c and the mean collision time T_c, respectively. Obviously, they are not appropriate as the characteristic scales for flow field in the continuum limit. Let the characteristic length scale of the flow field be L and let the characteristic flow speed be U. Moreover let the characteristic diffusion speed be W, which does coincide in general with U. There are two factors in the limit we are interested in. The continuum limit means $l_c \ll L$ and the low speed limit means $U \ll C$, where $C \, (= l_c/T_c)$ is the average modulus of the particle speed. In the following asymptotic analysis, we introduce the other dimensionless variables, defined by

$$x_i = (l_c/L)\hat{x}_i, \qquad t = (UT_c/L)\hat{t}. \tag{18}$$

Defining the small parameter ϵ as $\epsilon = l_c/L$, which corresponds to the Knudsen number, i.e. $\text{Kn} = \epsilon$, we have $x_i = \epsilon \hat{x}_i$. Furthermore, assuming the low Mach number limit [39], namely

$$\text{Ma} = U/C = \text{Kn} = l_c/L = \epsilon, \tag{19}$$

where Ma is the Mach number, we have $t = \epsilon^2 \hat{t}$. Then, Eq. (1) is rewritten as

$$\epsilon^2 \frac{\partial f_\sigma}{\partial t} + \epsilon V_i \frac{\partial f_\sigma}{\partial x_i} = \lambda \left[f_{\sigma(*)} - f_\sigma \right], \tag{20}$$

9

In this new scaling, we can assume

$$\frac{\partial f}{\partial \alpha} = O(f), \qquad \frac{\partial \hat{m}}{\partial \alpha} = O(\hat{m}), \tag{21}$$

where $f = f_{\sigma(*)}, f_\sigma$ and $\alpha = t, x_i$ and $\hat{m} = \hat{\rho}_\sigma, \hat{q}_{\sigma i}$.

2. Grad moment system

The key point of this section is to derive the macroscopic equations and, consequently, the definitions of the recovered transport coefficients. Let us introduce the general nomenclature for non-conserved equilibrium moments

$$\Pi^*_{(11\cdots1)_n\,(22\cdots2)_m} = \langle V_1^n V_2^m f_{\sigma(*)} \rangle. \tag{22}$$

Recalling that the diffusive scaling implies $\hat{u}_{\sigma i} = \epsilon\, u_{\sigma i}$ and $\hat{u}^*_{\sigma i} = \epsilon\, u^*_{\sigma i}$, a complete set of linearly independent moments is

$$
m_{\sigma(*)} =
\begin{bmatrix}
\Pi^* \\
\Pi^*_1 \\
\Pi^*_2 \\
\Pi^*_{11} \\
\Pi^*_{22} \\
\Pi^*_{12} \\
\Pi^*_{221} \\
\Pi^*_{112} \\
\Pi^*_{1122}
\end{bmatrix}
=
\begin{bmatrix}
\hat{\rho}_\sigma \\
\epsilon\,\hat{\rho}_\sigma u^*_{\sigma 1} \\
\epsilon\,\hat{\rho}_\sigma u^*_{\sigma 2} \\
\hat{p}_\sigma + \epsilon^2\,\hat{\rho}_\sigma (u^*_{\sigma 1})^2 \\
\hat{p}_\sigma + \epsilon^2\,\hat{\rho}_\sigma (u^*_{\sigma 2})^2 \\
\epsilon^2\,\hat{\rho}_\sigma u^*_{\sigma 1} u^*_{\sigma 2} \\
\epsilon\,\hat{\rho}_\sigma u^*_{\sigma 1}/3 \\
\epsilon\,\hat{\rho}_\sigma u^*_{\sigma 2}/3 \\
\hat{p}_\sigma/3 + \epsilon^2\,\hat{\rho}_\sigma (u^*_{\sigma 1})^2/3 + \epsilon^2\,\hat{\rho}_\sigma (u^*_{\sigma 2})^2/3
\end{bmatrix}. \tag{23}
$$

The previous nomenclature can be expressed for non-conserved generic moments as well, namely

$$\Pi_{(11\cdots1)_n\,(22\cdots2)_m} = \langle V_1^n V_2^m f_\sigma \rangle. \tag{24}$$

We can now apply the asymptotic analysis of the LB scheme based on the Grad moment system. Let us compute the first moments of the Eq. (20), namely

$$\frac{\partial \hat{\rho}_\sigma}{\partial t} + \frac{\partial (\hat{\rho}_\sigma u_{\sigma i})}{\partial x_i} = 0, \tag{25}$$

$$\epsilon^3 \frac{\partial (\hat{\rho}_\sigma u_{\sigma i})}{\partial t} + \epsilon \frac{\partial \Pi_{ij}}{\partial x_j} = \lambda (\Pi^*_i - \Pi_i) = \lambda \hat{\rho}_\sigma (\hat{u}^*_{\sigma i} - \hat{u}_{\sigma i}) = \hat{p} \sum_\varsigma B_{\sigma\varsigma}\, \hat{y}_\sigma \hat{y}_\varsigma (\hat{u}_{\varsigma i} - \hat{u}_{\sigma i}), \tag{26}$$

10

where Π_{ij} is the second-order moments tensor, $\hat{y}_\sigma = \hat{p}_\sigma/\hat{p}$ is the molar concentration and the relation $m\,\hat{x}_\sigma/m_\sigma = \hat{y}_\sigma$ has been used. In deriving the previous equations, the definitions given by Eq. (14) have been considered.

First of all, it is worth the effort to point out that the forcing terms in the previous equations are consistent with the macroscopic Maxwell–Stefan mass diffusion model. However the scaling of these forcing terms is not trivial in general. In the above mentioned Ref. [33] (see discussion after Eq. (27) of Ref. [33]), it was assumed that $u^*_{\sigma i} - u_{\sigma i} \sim O(1)$, or equivalently that $\hat{u}^*_{\sigma i} - \hat{u}_{\sigma i} \sim O(U/C) = O(\epsilon)$ (see Eq. (19)), which is equivalent to say that the constant U properly characterizes also the order of magnitude of the diffusion velocities. Hence the diffusion velocities are large, because they are of the same order of magnitude of the flow speed. In the following derivation, a more general approach is proposed.

Let us introduce the diffusion velocity, namely

$$\hat{w}_{\sigma i} = \hat{u}_{\sigma i} - \hat{v}_i, \tag{27}$$

where $\hat{v}_i = \sum_\sigma \hat{y}_\sigma \hat{u}_{\sigma i}$ is the mole–averaged mixture velocity. Let us assume that the quantity W is the proper characteristic diffusion speed, namely

$$\hat{w}_{\sigma i} = \frac{W}{C}\,w_{\sigma i} = \epsilon^{1+\beta}\,w_{\sigma i}, \tag{28}$$

where ϵ^β describes the ratio between diffusion and flow speed, namely $\epsilon^\beta = W/U$. Introducing the previous assumption into Eq. (26) yields

$$\epsilon^3 \frac{\partial(\hat{\rho}_\sigma u_{\sigma i})}{\partial t} + \epsilon \frac{\partial \Pi_{ij}}{\partial x_j} = \lambda(\Pi^*_i - \Pi_i) = \epsilon^{1+\beta}\,\hat{p}\sum_\varsigma B_{\sigma\varsigma}\,\hat{y}_\sigma \hat{y}_\varsigma (w_{\varsigma i} - w_{\sigma i}), \tag{29}$$

Clearly $\beta = 0$ corresponds to the case discussed in Ref. [33]. On the other hand, it is important to find out which value of β, i.e. which ratio between the diffusion and the flow velocity, is assumed by the expansion reported in the original paper by Andries, Aoki and Perthame [32]. The Chapman-Enskog expansion is a two-scale expansion considering both diffusive and advective scales, while here we focus on the diffusive scale only. However as far as the spatial gradients of the partial pressures are concerned, the difference among the two scales is unessential (both scales assume the spatial gradients proportional to the Knudsen number). The spatial gradients of the partial pressures are involved in the last term in the left-hand-side of Eq. (5.2) of Ref. [32], which is the single species momentum equation.

11

As usual, the spatial gradients of the partial pressures are scaled proportionally to $\mathrm{Kn}\,\mathrm{Ma}^2$: hence $W/C = \mathrm{Kn}\,\mathrm{Ma}^2$. Since $U/C = \mathrm{Ma}$, it follows that

$$W/U = \epsilon^\beta = \mathrm{Kn}\,\mathrm{Ma}. \tag{30}$$

This means that, as far as the Knudsen number is small and the Mach number is fixed, the diffusion speed is always smaller than the flow speed. In the present case, taking into account the diffusive scaling given by Eq. (19), the previous assumption yields $\beta = 2$. In the following, for taking into account both extreme cases, we assume $0 \le \beta \le 2$ in general.

In the momentum equation, the second-order moments tensor Π_{ij} appears. We now search for simplified expressions of the Π_{ij} tensor components. The equations for the Π_{ij} tensor components, namely

$$\epsilon^2 \frac{\partial \Pi_{ij}}{\partial t} + \epsilon \frac{\partial \Pi_{ijk}}{\partial x_k} = \lambda \left(\Pi_{ij}^* - \Pi_{ij} \right), \tag{31}$$

involve higher order moments like Π_{ijk}. The equations for Π_{ijk} can be simplified because of the lattice constraints (essentially $V_1^3 = V_1$ and $V_2^3 = V_2$). In fact $\Pi_{111} = \Pi_1 = \epsilon\,\hat{\rho}_\sigma u_{\sigma 1}$ and $\Pi_{222} = \Pi_2 = \epsilon\,\hat{\rho}_\sigma u_{\sigma 2}$. Moreover the equations for the remaining components are

$$\epsilon^2 \frac{\partial \Pi_{112}}{\partial t} + \epsilon \frac{\partial \Pi_{12}}{\partial x_1} + \epsilon \frac{\partial \Pi_{1122}}{\partial x_2} = \lambda \left(\Pi_{112}^* - \Pi_{112} \right), \tag{32}$$

$$\epsilon^2 \frac{\partial \Pi_{122}}{\partial t} + \epsilon \frac{\partial \Pi_{1122}}{\partial x_1} + \epsilon \frac{\partial \Pi_{12}}{\partial x_2} = \lambda \left(\Pi_{122}^* - \Pi_{122} \right). \tag{33}$$

Finally the equation for Π_{1122} is

$$\epsilon^2 \frac{\partial \Pi_{1122}}{\partial t} + \epsilon \frac{\partial \Pi_{122}}{\partial x_1} + \epsilon \frac{\partial \Pi_{112}}{\partial x_2} = \lambda \left(\Pi_{1122}^* - \Pi_{1122} \right). \tag{34}$$

In the continuum limit, each moment dynamics is ruled by its equilibrium part or eventually terms not larger than the equilibrium part. In case of the third order moments, the equilibrium part is

$$\Pi_{ijk}^* = \epsilon/3 \left(\delta_{ij}\hat{\rho}_\sigma u_{\sigma k}^* + \delta_{ki}\hat{\rho}_\sigma u_{\sigma j}^* + \delta_{jk}\hat{\rho}_\sigma u_{\sigma i}^* \right). \tag{35}$$

It is worth to point out that in the previous expression the density $\hat{\rho}_\sigma$ appears instead of the partial pressure $\hat{p}_\sigma$, as it would be required to recover the full isothermal macroscopic equations. This is certainly a limitation of the assumed local equilibrium given by Eq. (10), but it is acceptable as far as the low Mach number flows are concerned. In order to avoid such limitation on a stadard lattice, it is possible to use different meshes tailored on different

speeds of sound [27, 35] and to use some additional corrective terms in the local equilibrium [29]. Hence $O(\Pi_{ijk}) = O(\Pi^*_{ijk}) = O(\epsilon)$ and introducing this result into Eqs. (31) and into Eq. (34) yields

$$\Pi_{ij} - \Pi^*_{ij} = O(\epsilon^2), \tag{36}$$

$$\Pi_{1122} - \Pi^*_{1122} = O(\epsilon^2). \tag{37}$$

Taking into account that $\Pi^*_{ij} - \hat{p}_\sigma \delta_{ij} = O(\epsilon^2)$ and $\Pi^*_{1122} - \hat{p}_\sigma/3 = O(\epsilon^2)$, the previous expressions yield $\Pi_{ij} - \hat{p}_\sigma \delta_{ij} = O(\epsilon^2)$ and $\Pi_{1122} - \hat{p}_\sigma/3 = O(\epsilon^2)$. These expressions prove that the leading parts of Π_{11}, Π_{22} and Π_{1122} (all even) are ruled by $\hat{p}_\sigma$. Introducing the following expansion $\Pi_{ij} = \hat{p}_\sigma \delta_{ij} + \Pi^{(2)}_{ij} \epsilon^2$ into Eq. (29) yields

$$\frac{\partial \hat{p}_\sigma}{\partial x_i} = \epsilon^\beta \hat{p} \sum_\varsigma B_{\sigma\varsigma} \hat{y}_\sigma \hat{y}_\varsigma (w_{\varsigma i} - w_{\sigma i}) - \epsilon^2 \left[\frac{\partial(\hat{\rho}_\sigma u_{\sigma i})}{\partial t} + \frac{\partial \Pi^{(2)}_{ij}}{\partial x_j} \right]. \tag{38}$$

The previous equation allows one to discuss the proper scaling for the pressure $\hat{p}_\sigma$. Clearly two driving forces exist in the previous equation: the term $O(\epsilon^\beta)$ which describes the mass diffusion (according to the Maxwell–Stefan model) and the terms $O(\epsilon^2)$ which describe the viscous phenomena. Hence the most general expression for the single component pressure is $\hat{p}_\sigma = p^0_\sigma + \epsilon^\beta p'_\sigma + \epsilon^2 p''_\sigma$, where p^0_σ is an uniform field, i.e. $p^0_\sigma = p^0_\sigma(t)$. The previous conclusion yields consequently $\hat{\rho}_\sigma = \rho^0_\sigma + \epsilon^\beta \rho'_\sigma + \epsilon^2 \rho''_\sigma$, where ρ^0_σ is an uniform field, i.e. $\rho^0_\sigma = \rho^0_\sigma(t)$. With other words, it is possible to imagine that the single component pressure field $\hat{p}_\sigma$ is due to two contributions: a *slow* dynamics (in case $0 \leq \beta < 2$) mainly driven by the diffusion process p'_σ and a *fast* dynamics driven by the viscous phenomena p''_σ. Obviously in case $\beta = 2$, the two driving forces have a similar dynamics. These considerations lead to

$$\frac{\partial p'_\sigma}{\partial x_i} = \hat{p} \sum_\varsigma B_{\sigma\varsigma} \hat{y}_\sigma \hat{y}_\varsigma (w_{\varsigma i} - w_{\sigma i}), \tag{39}$$

$$\frac{\partial(\hat{\rho}_\sigma u_{\sigma i})}{\partial t} + \frac{\partial \Pi^{(2)}_{ij}}{\partial x_j} + \frac{\partial p''_\sigma}{\partial x_i} = 0, \tag{40}$$

Hence the *slow* dynamics p'_σ is driven by the diffusion process described by Eq. (39), while the *fast* dynamics p''_σ is driven by the viscous phenomena described by Eq. (40).

The next step is to search for a simplified expression for $\Pi^{(2)}_{ij}$. Introducing the previous

expansions for even moments into Eqs. (32-33) yields

$$\Pi_{112} = \frac{\epsilon}{3}\left(\hat{\rho}_\sigma u_{\sigma 2}^* - \frac{\epsilon^\beta}{\lambda}\frac{\partial p_\sigma'}{\partial x_2}\right) + O(\epsilon^3), \tag{41}$$

$$\Pi_{122} = \frac{\epsilon}{3}\left(\hat{\rho}_\sigma u_{\sigma 1}^* - \frac{\epsilon^\beta}{\lambda}\frac{\partial p_\sigma'}{\partial x_1}\right) + O(\epsilon^3). \tag{42}$$

Recalling that Eq. (39) is equivalent to $\partial p_\sigma'/\partial x_i = \lambda\hat{\rho}_\sigma(u_{\sigma i}^* - u_{\sigma i})$, the previous expressions become

$$\Pi_{112} = \frac{\epsilon}{3}\hat{\rho}_\sigma u_{\sigma 2} + O(\epsilon^3), \tag{43}$$

$$\Pi_{122} = \frac{\epsilon}{3}\hat{\rho}_\sigma u_{\sigma 1} + O(\epsilon^3). \tag{44}$$

Recalling that $\Pi_{ij} = \hat{p}_\sigma\delta_{ij} + \Pi_{ij}^{(2)}\epsilon^2$ and introducing the previous expressions into Eq. (31) yields

$$\Pi_{ij}^{(2)} = \hat{\rho}_\sigma u_{\sigma i}^* u_{\sigma j}^* - \nu\left[\frac{\partial(\hat{\rho}_\sigma u_{\sigma i})}{\partial x_j} + \frac{\partial(\hat{\rho}_\sigma u_{\sigma j})}{\partial x_i}\right] + (\nu - \xi_\sigma)\frac{\partial(\hat{\rho}_\sigma u_{\sigma k})}{\partial x_k}\delta_{ij} + O(\epsilon^2), \tag{45}$$

where the definitions given by Eqs. (15,16) have been used. Taking the divergence of the previous tensor yields

$$\frac{\partial\Pi_{ij}^{(2)}}{\partial x_j} = \frac{\partial}{\partial x_j}(\hat{\rho}_\sigma u_{\sigma i}^* u_{\sigma j}^*) - \nu\frac{\partial^2(\hat{\rho}_\sigma u_{\sigma i})}{\partial x_j^2} - \xi_\sigma\frac{\partial^2(\hat{\rho}_\sigma u_{\sigma k})}{\partial x_i\partial x_k} + O(\epsilon^2). \tag{46}$$

Recalling that

$$u_{\sigma i}^* u_{\sigma j}^* = u_i u_j + O(\epsilon^\beta), \tag{47}$$

$$\frac{\partial(\hat{\rho}_\sigma u_{\sigma k})}{\partial x_k} = -\epsilon^\beta\frac{\partial\rho_\sigma'}{\partial t} - \epsilon^2\frac{\partial\rho_\sigma''}{\partial t} = O(\epsilon^\beta), \tag{48}$$

yields

$$\frac{\partial\Pi_{ij}^{(2)}}{\partial x_j} = \frac{\partial}{\partial x_j}(\hat{\rho}_\sigma u_i u_j) - \nu\frac{\partial^2(\hat{\rho}_\sigma u_{\sigma i})}{\partial x_j^2} + O(\epsilon^\beta). \tag{49}$$

Introducing Eq. (49) into Eq. (40) yields

$$\frac{\partial(\hat{\rho}_\sigma u_{\sigma i})}{\partial t} + \frac{\partial}{\partial x_j}(\hat{\rho}_\sigma u_i u_j) + \frac{\partial p_\sigma''}{\partial x_i} = \nu\frac{\partial^2(\hat{\rho}_\sigma u_{\sigma i})}{\partial x_j^2} + O(\epsilon^\beta). \tag{50}$$

Introducing $\hat{\rho}_\sigma = \rho_\sigma^0 + \epsilon^\beta\rho_\sigma' + \epsilon^2\rho_\sigma''$ into Eq. (50) yields

$$\rho_\sigma^0\left[\frac{\partial u_{\sigma i}}{\partial t} + \frac{\partial}{\partial x_j}(u_i u_j) - \nu\frac{\partial^2 u_{\sigma i}}{\partial x_j^2}\right] + \frac{\partial p_\sigma''}{\partial x_i} = O(\epsilon^\beta). \tag{51}$$

14

Let us analyze the mixture dynamics. Summing over the components Eqs. (25), Eqs. (39) and Eqs. (50) yields

$$\frac{\partial \hat{\rho}}{\partial t} + \frac{\partial (\hat{\rho} u_i)}{\partial x_i} = 0, \tag{52}$$

$$\frac{\partial p'}{\partial x_i} = 0, \tag{53}$$

$$\frac{\partial (\hat{\rho} u_i)}{\partial t} + \frac{\partial}{\partial x_j}(\hat{\rho} u_i u_j) + \frac{\partial p''}{\partial x_i} = \nu \frac{\partial^2 (\hat{\rho} u_i)}{\partial x_j^2} + O(\epsilon^\beta), \tag{54}$$

where $p' = \sum_\sigma p'_\sigma$ and $p'' = \sum_\sigma p''_\sigma$. From Eq. (53), one gets that the leading pressure field is uniform, i.e. $p' = p'(t)$, which can be included into $p^0(t) = \sum_\sigma p^0_\sigma(t)$. Hence $\hat{p} = p^0(t) + \epsilon^2 p''$ and consequently $\hat{\rho} = \rho^0(t) + \epsilon^2 \rho''$, where $O(p'') = O(\rho'') = 1$. In case of the single species dynamics, the *slow* dynamics p'_σ is driven by the diffusion process described by Eq. (39), while the *fast* dynamics p''_σ is driven by the viscous phenomena described by Eq. (40). In case of the mixture, only the viscous phenomena remain, where the *fast* dynamics p'' is driven by Eq. (54). However there is no *slow* dynamics for the mixture (i.e. the mixture momentum is conserved). This means that, at the leading diffusion order, single species pressure fields characterized by large gradients are possible, as far as their net effect is a nearly uniform total pressure field (otherwise the non-smooth total pressure field would produce accelerations which are not compatible with the low Mach number limit).

Including the expansion $\hat{\rho} = \rho^0(t) + \epsilon^2 \rho''$ into Eq. (52) yields

$$\frac{1}{\rho^0}\frac{d\rho^0}{dt} + \frac{\partial u_i}{\partial x_i} = O(\epsilon^2), \tag{55}$$

and integrating the previous on the considered domain Ω yields

$$\frac{1}{\rho^0}\frac{d\rho^0}{dt} = -\left(\int_\Omega dx_1 dx_2\right)^{-1}\int_{\partial\Omega}(u_i n_i)\,ds + O(\epsilon^2), \tag{56}$$

where $\partial\Omega$ is the border of the domain Ω, ds is the line element and n_i is the component of the unit vector normal to ds and pointing in the outward direction. In the following, let us restrict ourselves to boundary conditions for the total mixture velocity such that

$$\int_{\partial\Omega}(u_i n_i)\,ds = O(\epsilon^2). \tag{57}$$

The previous condition is the typical compatibility condition for incompressible flows (see the analysis reported in Appendix A.2 of Ref. [46] for the single species case). Introducing

15

the assumption given by Eq. (57) into Eq. (56) yields the following expansion $\rho^0(t) = \rho_0^0 + \epsilon^2 \rho_t^0(t)$, where ρ_0^0 is a constant and $\rho_t^0 = \rho_t^0(t)$ is another uniform function. Including $\rho_t^0(t)$ into ρ'' yields $\hat{\rho} = \rho_0^0 + \epsilon^2 \rho''$ and similarly $\hat{p} = p_0^0 + \epsilon^2 p''$. Finally, recalling that $O(p'') = O(\rho'') = 1$, Eqs. (52, 54) become

$$\frac{\partial u_i}{\partial x_i} = O(\epsilon^2), \tag{58}$$

$$\rho_0^0 \left[\frac{\partial u_i}{\partial t} + u_j \frac{\partial u_i}{\partial x_j} - \nu \frac{\partial^2 u_i}{\partial x_j^2} \right] + \frac{\partial p''}{\partial x_i} = O(\epsilon^\beta). \tag{59}$$

Clearly the previous equations are the canonical Navier–Stokes system of equations in the incompressible limit for the barycentric velocity u_i, in case $0 < \beta \leq 2$. The case $\beta = 0$ must be excluded, because it does not recover the Navier-Stokes equations, as already pointed out in Ref. [33]. Hence, from the numerical point of view, the scheme is second order with regards to ϵ, in the original case considered by Andries, Aoki and Perthame [32], i.e. $\beta = 2$, while it is only first order in case of larger diffusion velocities, i.e. $\beta = 1$. It is worth to point out that the latter case corresponds to larger diffusion speed, but anyway one order of magnitude smaller than flow speed ($W/U = \epsilon$).

Equations (58, 59) are fully decoupled from any diffusion dynamics since the pressure p'' in Eq. (59) is not defined by any thermodynamic relation but by the incompressibility condition given by Eq. (58). This is not surprising because, in the incompressible limit, any information abut the thermodynamic equation of state is entirely lost when describing the diffusion effects described by p''.

Hence let us investigate how the pressure p'' effects the complete diffusion equation. Recalling that $u_{\sigma i} - u_i = O(\epsilon^\beta)$ and combining Eqs. (51) and Eqs. (59) yields

$$\frac{\partial p_\sigma''}{\partial x_i} = \frac{\rho_\sigma^0}{\rho_0^0} \frac{\partial p''}{\partial x_i} + O(\epsilon^\beta) = \hat{x}_\sigma \frac{\partial p''}{\partial x_i} + O(\epsilon^\beta), \tag{60}$$

because $\rho_\sigma^0/\rho_0^0 = \hat{x}_\sigma + O(\epsilon^\beta)$. The previous relation suggests that the *fast* mode dynamics p_σ'' is ruled by the total pressure dynamics p'': hence the p_σ'' can be defined the barycentric contribution or better the barodiffusion term. The previous expression is equivalent to that reported in Lemma 4.4 of Ref. [32], with the difference that now p'' is defined by incompressibility condition rather that by thermodynamics as in Ref. [32], where the full compressible case is considered. Multiplying Eq. (39) by ϵ^β, Eq. (60) by ϵ^2, summing the

16

results and dividing by $\hat{p}$ yields

$$\frac{1}{\hat{p}}\frac{\partial \hat{p}_\sigma}{\partial x_i} = \sum_\varsigma B_{\sigma\varsigma}\,\hat{y}_\sigma\hat{y}_\varsigma(u_{\varsigma i} - u_{\sigma i}) + \frac{\hat{x}_\sigma}{\hat{p}}\frac{\partial \hat{p}}{\partial x_i} + O(\epsilon^{2+\beta}), \qquad (61)$$

and consequently

$$\frac{\partial \hat{y}_\sigma}{\partial x_i} = \sum_\varsigma B_{\sigma\varsigma}\,\hat{y}_\sigma\hat{y}_\varsigma(u_{\varsigma i} - u_{\sigma i}) + \frac{(\hat{x}_\sigma - \hat{y}_\sigma)}{\hat{p}}\frac{\partial \hat{p}}{\partial x_i} + O(\epsilon^{2+\beta}). \qquad (62)$$

In the previous expression, the barodiffusion term depends on the mixture pressure $\hat{p}$, however the latter (in this asymptotic limit) depends only on the hydrodynamic pressure p'', which is ruled by the incompressibility condition. The latter effect is a direct consequence of the incompressible description of the mixture fluid dynamics. Once the terms $O(\epsilon^{2+\beta})$ are neglected, the previous formula represents the standard Maxwell–Stefan model, which contains two terms in the present situation: the component diffusion due to differences in single species velocities and the barodiffusion term [30].

In the next section, some details are reported concerning the macroscopic mass diffusion modeling.

C. Macroscopic modeling

Before proceeding with the numerical implementation of the LBM scheme, some issues are reported concerning the macroscopic mass diffusion modeling, in particular in case of more than two components.

First of all, Eq. (39) can be equivalently written as

$$-\frac{1}{y_\sigma}\frac{\partial y_\sigma}{\partial x_i} = \sum_{\varsigma \neq \sigma} B_{\sigma\varsigma}\,y_\varsigma(u_{\sigma i} - u_{\varsigma i}), \qquad (63)$$

which is the canonical form of the Maxwell–Stefan mass diffusion model. Introducing some proper coefficients $C_{\sigma i}$ such that

$$y_\sigma(u_{\sigma i} - u_i) = -C_{\sigma i}\frac{\partial y_\sigma}{\partial x_i}, \qquad (64)$$

and substituting them into Eq. (63) yields

$$-\frac{1}{y_\sigma}\frac{\partial y_\sigma}{\partial x_i} = \sum_{\varsigma \neq \sigma} B_{\sigma\varsigma}\,y_\varsigma(u_{\sigma i} - u_{\varsigma i}) = \frac{1}{C_{\sigma i}}\sum_{\varsigma \neq \sigma} x_\varsigma(u_{\sigma i} - u_{\varsigma i}). \qquad (65)$$

17

Assuming that there is already good mixing among the remaining species, namely $u_{\varsigma i} \approx u_{0i}$ (where u_{0i} is sometimes called carrier velocity) for all $\varsigma \neq \sigma$, yields the so-called mixture averaged diffusion approximation (MADA) [30], namely

$$C_{\sigma i} \approx C_{\sigma 0} = \frac{1 - x_\sigma}{\sum_{\varsigma \neq \sigma} B_{\sigma \varsigma} \, y_\varsigma}. \tag{66}$$

It is worth to point out that MADA is different from assuming small diffusion speed. MADA concerns all species ς but σ, while small diffusion speed means that all the species evolve close to the barycentric mixture velocity (and in general $u_i \neq u_{0i}$). Introducing the definition given by Eq. (64) and the MADA given by Eq. (66) into Eq. (25) yields

$$\frac{\partial y_\sigma}{\partial t} + \frac{\partial (y_\sigma u_i)}{\partial x_i} = \nabla \cdot (C_{\sigma 0} \nabla y_\sigma), \tag{67}$$

which is an advection-diffusion equation (ADE) with an effective transport coefficient $C_{\sigma 0}$, ruling the diffusion of the molar concentration y_σ. It is worth to point out that the LBM scheme solves directly Eq. (63) without any additional approximation, while the most popular macroscopic approach is based on Eq. (67) which requires the MADA given by Eq. (66).

In the next section, some details about the numerical implementation are reported.

D. Efficient numerical implementation

In the previous sections, the space–time discretization has not been discussed. It is well known that it is very convenient to discretize the LBM schemes along the characteristics, i.e. along the lattice velocities, because they are constant and analytically known. However the popular forward Euler integration rule can not be applied in this case because it leads to a lack of mass conservation [26]. Essentially in case of large pressure gradients, the discrete numerical effects appear also in the continuity equation. For proving this, it is enough to consider the Taylor expansion of the standard Lattice Boltzmann scheme and to apply the definition of the zeroth order moment. The final macroscopic equation would depend on the Laplacian of the pressure field, which may work as an artificial source term in the continuity equation, in case of large pressure gradients.

Consequently a more accurate scheme must be considered: for example, the second-order Crank–Nicolson rule is enough in order to avoid this problem. In the following, the SRT

formulation will be considered only: the generalization of the numerical implementation in case of multiple relaxation frequencies is discussed in Ref. [40].

Let us discretize Eq. (20) by the following formula

$$f_\sigma^+ = f_\sigma + (1 - \theta)\,\lambda\left[f_{\sigma(*)} - f_\sigma\right] + \theta\,\lambda^+\left[f_{\sigma(*)}^+ - f_\sigma^+\right], \tag{68}$$

where the argument (t, x_i) is omitted and the functions computed in $(t + \epsilon^2, x_i + \epsilon V_i)$ are identified by the superscript $+$. The Crank–Nicolson rule is recovered for $\theta = 1/2$. The previous formula would force one to consider quite complicated integration procedures [26]. Fortunately a simple variable transformation has been already proposed in order to simplify this task [42], and successfully applied in case of mixtures [27, 28]. The generalization of this procedure in case of multiple relaxation frequencies is trivial by following Ref. [43].

Let us introduce a local transformation

$$g_\sigma = f_\sigma - \theta\,\lambda\left[f_{\sigma(*)} - f_\sigma\right]. \tag{69}$$

Substituting the transformation given by Eq. (69) into Eq. (68) yields

$$g_\sigma^+ = g_\sigma + \frac{\lambda}{1 + \theta\lambda}\left[f_{\sigma(*)} - g_\sigma\right], \tag{70}$$

where it is worth to remark that the local equilibrium remains unchanged. Essentially the algorithm consisists of (a) appling the previous transformation $f_\sigma \to g_\sigma$ defined by Eq. (69), then (b) computing the collision step $g_\sigma \to g_\sigma^+$ by means of the formula given by Eq. (70) and finally (c) coming back to the original discrete distribution function $g_\sigma^+ \to f_\sigma^+$. The problem, in case of mixtures, arises from the last step. In fact, the formula required in order to perform the last task (c) is

$$f_\sigma^+ = \frac{g_\sigma^+ + \theta\,\lambda^+ f_{\sigma(*)}^+}{1 + \theta\,\lambda^+}. \tag{71}$$

In order to compute both λ^+ (depending on total pressure and total density) and $f_{\sigma(*)}^+$, the updated hydrodynamic moments, i.e. the hydrodynamic moments at the new time step, are required. Since the single component density is conserved, recalling Eq. (69) yields

$$\rho_\sigma^+ = \langle g_\sigma^+ \rangle, \tag{72}$$

consequently it is possible to compute p_σ^+, ρ^+, p^+ and finally λ^+.

However this is not the case for the single component momentum, because this is not a conserved quantity and hence the first order moments for g_σ^+ and f_σ^+ differ [27, 28]. Recalling Eq. (69) and taking the first order moment of it yields

$$\langle V_i\, g_\sigma^+ \rangle = \rho_\sigma^+ u_{\sigma i}^+ - \theta\,\lambda^+ \rho_\sigma^+ (u_{\sigma i}^{*+} - u_{\sigma i}^+) = \rho_\sigma^+ u_{\sigma i}^+ - \theta\, p^+ \sum_\varsigma B_{\sigma\varsigma}\, y_\sigma^+ y_\varsigma^+ (u_{\varsigma i}^+ - u_{\sigma i}^+). \qquad (73)$$

It is worth to point out an important property. Summing the previous equations for all the components yields

$$\sum_\sigma \langle V_i\, g_\sigma^+ \rangle = \rho^+ u_i^+, \qquad (74)$$

which means that, since the total mixture momentum is conserved, then it is possible to compute it directly by means of g_σ^+. For this reason, it is possible to consider a simplified procedure in case of particles with similar masses.

1. Particles with similar masses

In case of particles with similar masses, $u_{\sigma i}^{*+} \approx u_i^+$ and Eq. (73) reduces to

$$\langle V_i\, g_\sigma^+ \rangle \approx \rho_\sigma^+ u_{\sigma i}^+ - \theta\,\lambda^+ \rho_\sigma^+ (u_i^+ - u_{\sigma i}^+), \qquad (75)$$

and equivalently, by taking into account Eq. (74),

$$\rho_\sigma^+ u_{\sigma i}^+ \approx \frac{\langle V_i\, g_\sigma^+ \rangle + \theta\,\lambda^+ x_\sigma^+ \sum_\sigma \langle V_i\, g_\sigma^+ \rangle}{1 + \theta\,\lambda^+}. \qquad (76)$$

Actually the situation is even simpler, bacause the previous formula is not needed. In fact, if $u_{\sigma i}^{*+} \approx u_i^+$, it is enough u_i^+ by Eq. (74) to compute $f_{\sigma(*)}^+$ for the back transformation given by Eq. (71).

2. Particles with different masses

In the general case, Eq. (73) can be recasted as

$$\langle V_i\, g_\sigma^+ \rangle = q_{\sigma i}^+ - \theta\,\lambda^+ \sum_\varsigma \chi_{\sigma\varsigma}\, (x_\sigma^+ q_{\varsigma i}^+ - x_\varsigma^+ q_{\sigma i}^+), \qquad (77)$$

where $q_{\sigma i}^+ = \rho_\sigma^+ u_{\sigma i}^+$ and

$$\chi_{\sigma\varsigma} = \frac{m^2}{m_\sigma m_\varsigma} \frac{B_{\sigma\varsigma}}{B_{mm}}, \qquad (78)$$

is a symmetric matrix. Finally, grouping together common terms yields

$$\langle V_i\, g_\sigma^+ \rangle = \left[1 + \theta\, \lambda^+ \sum_\varsigma (\chi_{\sigma\varsigma}\, x_\varsigma^+) \right] q_{\sigma i}^+ - \theta\, \lambda^+\, x_\sigma^+ \sum_\varsigma (\chi_{\sigma\varsigma}\, q_{\varsigma i}^+). \qquad (79)$$

Clearly the previous expression defines a liner system of algebraic equations for the unknowns $q_{\sigma i}^+$. This means that in order to compute the updated values for all $q_{\sigma i}^+$ a linear system of equations must be solved in terms of known quantities $\langle V_i\, g_\sigma^+ \rangle$. Obviously the solvability condition for the previous system depends on the updated mass concentrations and it can not be ensured in general. Note that this potential restriction of the discussed scheme is a constraint of the proposed numerical implementation and not of the kinetic model itself. The possibility to tune θ is not available, because all the schemes for $\theta \neq 1/2$ may imply a lack of mass conservation. Even though this feature did not represent a problem in the reported numerical simulations, it should be further investigated.

In the degenerate case $\chi_{\sigma\varsigma} = 1$, i.e. particles with equal masses, Eq. (79) reduces to

$$\langle V_i\, g_\sigma^+ \rangle = \left(1 + \theta\, \lambda^+ \right) q_{\sigma i}^+ - \theta\, \lambda^+\, x_\sigma^+ q_i^+, \qquad (80)$$

which is equivalent to Eq. (76).

In the next section, the results for some numerical simulations are reported.

III.   NUMERICAL SIMULATIONS

A.   Fickian limiting test cases

In this paper, some simple numerical tests are considered, essentially concerning the recovered macroscopic diffusion model in the continuum limit, which represents the main improvement of the proposed scheme. In particular, the Maxwell–Stefan diffusion model, in comparison with the simpler Fick model, allows one to automatically recover the effective diffusion coefficients in different limiting cases, depending on the local concentrations, without any *a priori* guess about the concentration fields. In particular, in the reported numerical simulations, this feature will be verified in two limiting cases: (a) the solvent test case and (b) the dilute test case [34, 44]. The geometrical configuration and the procedure in order to measure the transport coefficients is quite standard [16, 35] and it can be physically explained as the mixing in an opposed-jet configuration [27].

21

In case of ternary mixture Eq. (63) reduces to

$$n\frac{\partial y_1}{\partial x_i} = B_{12}y_1k_{2i} + B_{13}y_1k_{3i} - (B_{12}y_2 + B_{13}y_3)k_{1i}, \tag{81}$$

$$n\frac{\partial y_2}{\partial x_i} = B_{21}y_2k_{1i} + B_{23}y_2k_{3i} - (B_{21}y_1 + B_{23}y_3)k_{2i}, \tag{82}$$

$$n\frac{\partial y_3}{\partial x_i} = B_{31}y_3k_{1i} + B_{32}y_3k_{2i} - (B_{31}y_1 + B_{32}y_2)k_{3i}, \tag{83}$$

where $k_{\sigma i} = n_\sigma(u_{\sigma i} - v_i)$ and $v_i = \sum_\sigma y_\sigma u_{\sigma i}$ is the mole–averaged mixture velocity. Let us consider a 1D computational domain, filled by a ternary mixture. All the physical quantities will be expressed in lattice units. The molecular weights are $m_\sigma = [1, 2, 3]$ and consequently the corrective factors are $\varphi_\sigma = [1, 1/2, 1/3]$.

The generalized Fick model can be expressed as

$$k_{\sigma i} = -nD_\sigma\frac{\partial y_\sigma}{\partial x_i}, \tag{84}$$

where D_σ is the Fick diffusion coefficient. Eq. (84) substantially differs from Eq. (64) because the latter involves the mass-averaged (barycentric) mixture velocity. In the numerical simulations, the theoretical Fick diffusion coefficient is $D_\sigma = c_D/m_\sigma$, where $c_D \in [0.002, 0.8]$ and the theoretical Maxwell–Stefan diffusion resistance [34] is given by

$$B_{\sigma\varsigma} = c_B \left(\frac{1}{m_\sigma} + \frac{1}{m_\varsigma}\right)^{-1/2}, \tag{85}$$

where $c_B \in [5, 166]$.

The computational domain is defined by $(t, x) \in [0, T] \times [0, L]$. The boundary conditions for all the components at the borders of the computational domain, i.e. at $x = 0, L$, are of Neumann type, i.e. $\partial p_\sigma/\partial x = 0$ at any time. The initial conditions depends on the considered limiting case (see below). The spatial discretization step is called δx and the total number of grid points is $N_x = L/\delta x = 100$. Similarly the time discretization step is selected in such a way that $\delta t \sim \delta x$ in order to have $C = \delta x/\delta t = 1$, and in particular $N_t = T/\delta t = 30$.

1. Solvent test case

A component of a mixture is called *solvent* if its concentration is predominant in comparison with the other components of the mixture. Let us suppose that, in our ternary mixture,

the component 3 is a solvent. In particular, the initial conditions for the solvent test case are given by

$$p_1(0, x) = \Delta p \left[1 + \tanh \left(\frac{x - L/2}{\delta x} \right) \right] + p_s, \tag{86}$$

$$p_2(0, x) = \Delta p \left[1 - \tanh \left(\frac{x - L/2}{\delta x} \right) \right] + p_s, \tag{87}$$

$$p_3(0, x) = 1 - 2 \left(\Delta p + p_s \right), \tag{88}$$

where clearly $p(0, x) = \sum_\sigma p_\sigma = 1$. In the reported numerical simulations, $\Delta p = p_s = 0.01$. The parameter p_s is a small pressure shift in order to avoid divisions by zero in passing from the momentum to the velocity.

Hence $y_3 \approx 1$ and consequently $y_1 \approx 0$ and $y_2 \approx 0$. Under these assumptions, Eqs. (81, 82) reduce to

$$\frac{\partial y_1}{\partial x} = -B_{13} y_1 (u_1 - v) = B_{13} y_1 (v - u_1), \tag{89}$$

$$\frac{\partial y_2}{\partial x} = -B_{23} y_2 (u_2 - v) = B_{23} y_2 (v - u_2), \tag{90}$$

Consequently the measured diffusion resistances are given by

$$B_{13}^* = \frac{1}{D_1^*} = \frac{\partial y_1 / \partial x}{y_1 (v - u_1)}, \tag{91}$$

$$B_{23}^* = \frac{1}{D_2^*} = \frac{\partial y_2 / \partial x}{y_2 (v - u_2)}, \tag{92}$$

where, since in this test, the Maxwell–Stefan model reduces to the Fick model, it is possible to define two Fick diffusion coefficients $D_1 = 1/B_{13}$ and $D_2 = 1/B_{23}$ for non-solvent components. Since the main attention was for the mass diffusion process, in the reported numerical results the SRT formulation was considered. For this reason, the viscous dynamics (next approximation of the mixture momentum equation) is not reliable. In particular, the SRT formulation does not allow one to relax all the single component stress tensors with the same mixture viscosity as it should be for recovering the mixture dynamics. This means that, for the reported simulations, the ratio between the Fick diffusion coefficient and the mixture viscosity $Sc = \nu/D$, i.e. the Schmidt number, is not reliable.

First of all, a generalized Fick model was implemented and the corresponding numerical results are reported in Figs. 1 and 2 for non-solvent component 1 and 2 respectively, for the measured transport coefficients at time $T = 30 \, \delta t$ and spatial location $x = L/2$. In case of the Fick model, a direct correlation exists between the Fick diffusion coefficient and

23

the relaxation frequency, namely $\lambda_\sigma = \varphi_\sigma/(3\,D_\sigma)$, and this explains the auxiliary axises of the previous figures. The implicit numerical implementation allows one to consider large relaxation frequencies, since the stability region is widened. The SRT implementation of the generalized Fick model well matches the expected transport coefficients. At the lowest and the highest end of the considered range, the measured transport coefficients slightly overestimate and underestimate the theoretical values respectively.

Secondly, a complete Maxwell–Stefan model, without *a priori* restriction of the mixture-averaged approximation [30, 34], was implemented and the corresponding numerical results are reported in Figs. 3 and 4 respectively. The key idea is to verify that the model automatically reduces to the solvent limit, i.e. that the dynamics of component 1 is mainly ruled by resistance B_{13} and that of component 2 by resistance B_{23}. In this case, there is no direct correlation between the Maxwell–Stefan resistances (three as the possible interacting couples) and the relaxation frequency $\lambda_\sigma = \lambda$ (one for the mixture, according to the proposed model). As the number of components increases, then the number of Maxwell–Stefan resistances is usually larger than the number of components. Also in this case, the SRT implementation of the Maxwell–Stefan model well matches the expected resistance coefficients.

2. Dilute test case

A component of a mixture is said *dilute* if its concentration is negligible in comparison with the other components of the mixture. Let us suppose that, in our ternary mixture, the component 1 is dilute. In particular, the initial conditions for the dilute test case are given by

$$p_1(0, x) = \Delta p \left[1 + \tanh\left(\frac{x - L/2}{\delta x}\right)\right] + p_s, \tag{93}$$

$$p_2(0, x) = \Delta p \left[1 - \tanh\left(\frac{x - L/2}{\delta x}\right)\right] + p_s + (1 - r)(1 - 2\,\Delta p), \tag{94}$$

$$p_3(0, x) = r(1 - 2\,\Delta p) - 2\,p_s, \tag{95}$$

where clearly $p(0, x) = \sum_\sigma p_\sigma = 1$. In the reported numerical simulations, $\Delta p = p_s = 0.01$ and $r = 1/2$. Clearly r must be close to $1/2$, otherwise this test case reduces to the previous one about existence of a solvent. Again the parameter p_s is a small pressure shift in order to avoid divisions by zero in passing from the momentum to the velocity.

Hence $y_1 \approx 0$ and consequently $y_1 \ll y_2 + y_3$. Under these assumptions, Eq. (81) reduces to

$$\frac{\partial y_1}{\partial x} = y_1 \, B_1 \, (v - u_1), \tag{96}$$

where $B_1 = B_{12}y_2 + B_{13}y_3$ is an equivalent effective resistance. Consequently the measured diffusion resistance is given by

$$B_1^* = \frac{1}{D_1^*} = \frac{\partial y_1/\partial x}{y_1(v - u_1)}, \tag{97}$$

where, since also in this test, the Maxwell–Stefan model reduces to the Fick model, it is possible to define a Fick diffusion coefficients $D_1 = 1/B_1$ for the dilute component. Concerning the actual Schmidt number, considerations similar to those already discussed for the previous test case holds here as well.

In Fig. 5, the numerical results for the Maxwell–Stefan implementation are reported and, in particular, the measured values for the equivalent effective resistance B_1 are compared with the theoretical expected values. Also in this case, the SRT implementation of the Maxwell–Stefan model well matches the expected values. It is worth to point out that the effective resistance B_1 is never directly imposed in the code, but it is a natural outcome of the model, which depends on the local molar concentrations.

B. Non-Fickian test case: Stefan tube

The previous numerical simulations proved that the proposed model allows one to recover some well-known results for Fickian test cases. Since there are already plenty of lattice Boltzmann implementations that simulate Fickian diffusion, the innovative part of the previous simulations relies on the fact that all the transport coefficients of the model are kept constant for all the tests, without introducing any artificial external tuning, in order to match the considered limiting test case.

In this section, the full capabilities of the Maxwell–Stefan model will be proved for a non-Fickian test case. Let us consider a popular test, i.e. the Stefan tube (see chapter 2 of [44] for details). The Stefan tube is a simple device sometimes used for measuring diffusion coefficients in binary vapor mixtures, in case of the presence of an additional gas carrier. It is essentially a vertical tube, open at one end, where the carrier flow licks orthogonally the tube opening. In the bottom of the tube is a pool of quiescent liquid. The vapor that

25

evaporates from this pool diffuses to the top of the tube. The stream of gas carrier across the top of the tube keeps the molar concentration of diffusing vapor there essentially to nothing. The molar concentration of the vapor at the vapor-liquid interface is its equilibrium value.

For sake of simplicity, let us consider the same ternary mixture, already discussed in the previous sections, where the third species is assumed to be the gas carrier. Let us assume Eq. (85) for the Maxwell–Stefan diffusion resistance, with $c_B = 66.13$, which implies $B_{13} = 57.27$, $B_{12} = 54.00$, $B_{23} = 72.44$.

The computational domain is defined by $(t, x) \in [0, T] \times [0, L]$. Concerning the boundary conditions, the partial pressures for all the species at the bottom of the tube $p_1(0, 0) = 0.319$, $p_2(0, 0) = 0.528$, $p_3(0, 0) = 0.1530$ and those at the opening of the tube $p_1(0, L) = 0.0$, $p_2(0, L) = 0.0$, $p_3(0, L) = 1.0$ are specified. In particular, the pressure condition proposed in Ref. [45] was adopted. This boundary condition is now available for the lattice Boltzmann method too [46]. Recasting this condition for the compressible case reads

$$-p_\sigma n_i + \nu \frac{\partial(\rho_\sigma u_{\sigma i})}{\partial n_i} = -\bar{p}_\sigma n_i, \tag{98}$$

where n_i is the component of the outer unit vector along the normal direction at the boundary, p_σ is the pressure at the boundary and $\bar{p}_\sigma$ is the average pressure at the boundary. In our mono-dimensional test case, clearly $\bar{p}_\sigma = p_\sigma$ and the previous condition implies $\partial(\rho_\sigma u_{\sigma 1})/\partial x = 0$ at both $x = 0, L$. This means that we have to consider both Dirichlet boundary conditions (for partial pressures) and homogeneous Neumann boundary conditions (for single species momenta).

The initial conditions are

$$p_1(0, x) = p_1(0, 0) \frac{1}{2} \left[1 - \tanh\left(\frac{x - L/2}{\delta x}\right) \right] + p_s, \tag{99}$$

$$p_2(0, x) = p_2(0, 0) \frac{1}{2} \left[1 - \tanh\left(\frac{x - L/2}{\delta x}\right) \right] + p_s, \tag{100}$$

$$p_3(0, x) = [1 - p_3(0, 0)] \frac{1}{2} \left[1 + \tanh\left(\frac{x - L/2}{\delta x}\right) \right] + p_3(0, 0), \tag{101}$$

where the constant $p_s = 10^{-4}$ has been introduced for stability reasons, i.e. for avoiding to divide per zero in the computation of the velocity.

The spatial discretization step is called δx and the total number of grid points is $N_x = L/\delta x = 60$. Similarly the time discretization step is selected in such a way that $\delta t \sim \delta x$ in order to have $C = \delta x/\delta t = 1$, and in particular $N_t = T/\delta t = 120, 000$.

Concerning the numerical solution, at constant temperature and pressure, the total molar density is constant and the driving forces are the molar concentration gradients ∇y_σ. Furthermore, since there are no radial or circumferential gradients in the composition, the continuity equation at steady state implies that $\rho_\sigma u_{\sigma 1}$ is a constant, as well as $N_\sigma = y_\sigma u_{\sigma 1}$. The first two Eqs. (81, 82) can be rewritten as

$$\frac{dy_1}{dx} = B_{12}(y_1 N_2 - y_2 N_1) + B_{13}[y_1 N_3 - (1 - y_1 - y_2)N_1], \tag{102}$$

$$\frac{dy_2}{dx} = B_{12}(y_2 N_1 - y_1 N_2) + B_{23}[y_2 N_3 - (1 - y_1 - y_2)N_2], \tag{103}$$

while Eq. (83) can be omitted, since it is not linearly independent on the previous ones. The previous system of ordinary differential equations, with the boundary conditions already discussed, realizes a boundary value problem, which can be solved, for example, by the shooting method [47]. Essentially the idea is to define the proper values for the parameters N_1, N_2, N_3 in order to ensure the required boundary conditions at $x = L$. The solution of this problem is not unique. In fact, some additional information concerning the physics of the problem needs to be provided. For example, from the practical point of view, usually the gas carrier does not dissolve in the liquid and, for this reason, its flux is zero, i.e. $N_3 = 0$. In general, the pressure difference across the tube of the gas carrier is responsible of its dynamics. Hence the flux of the gas carrier points toward the liquid pool at the bottom, i.e. $N_3 \leq 0$. In the following, two tests are reported with $N_3 = 0$ and $N_3 = -6.1776 \cdot 10^{-5}$ respectively.

In Figs. 6 and 7 the molar concentration profiles are reported for both cases. The numerical simulations performed by the proposed LBM model agree well with the results obtained by directly solving the boundary value problem. Clearly the molar concentrations show a non-Fickian behavior. In fact, the Fick model would prescribe linear profiles of the molar concentrations for this boundary value problem. The coupling among the species, which is responsible of the non linear profiles, can not be simulated by any simplified Fick diffusion coefficient. This feature, which has been experimentally proved by Carty and Schrodt (1975) [48], demonstrates the superiority of the Maxwell–Stefan formulation.

Concerning the LBM implementation of the model, special attention must be devoted to the partial pressure boundary conditions in a general application. For the reported results, a simple boundary condition in the moment space was adopted, but more complicated cases would required more accurate boundary conditions, like those reported in Ref. [46].

IV. CONCLUSIONS

In the present paper, a recently proposed LBM scheme for homogeneous mixture modeling [33], which recovers Maxwell–Stefan diffusion model in the continuum limit, without the restriction of the macroscopic mixture-averaged approximation [30], was analyzed. This scheme is derived from a popular BGK-type kinetic model for gas mixtures [32], even though the present LB formulation concerns only the incompressible isothermal limit. Hence the full potential advantage of this kinetic model is not completely inherited. However, for low Mach number flows, the LBM formulation correctly recovers the Maxwell–Stefan diffusion model in the standard form given by Eq. (62) and the incompressible Navier–Stokes equations given by Eqs. (58, 59). This means that, in the continuum limit, the present scheme solves a set of macroscopic fluid dynamic equations which are fully decoupled from species dynamics. Other LBM schemes have been proposed which present similar features, but introducing this decoupling from the very beginning in the kinetic equations. On the other hand, this paper investigates the decoupling of the diffusion and fluid dynamic equations, which is typical in the incompressible limit, starting from a reference kinetic model and for different scalings of the diffusion velocities, with regards to the flow velocities.

In the present paper, the recovered macroscopic equations in the continuum limit were systematically investigated by varying the ratio between characteristic diffusion speed (W) and characteristic barycentric speed (U), i.e. $W/U = \epsilon^{\beta}$. If the diffusive scaling is adopted, it comes out that the diffusion speed must be at least one order of magnitude (in terms of ϵ) smaller than the barycentric speed, in order to recover the correct Navier-Stokes equations for mixtures in the incompressible limit. The case $\beta = 0$ must be excluded, because it does not recover the Navier-Stokes equations, as already pointed out in Ref. [33]. Hence, from the numerical point of view, the scheme is second order with regards to ϵ, in the original case considered by Andries, Aoki and Perthame [32], i.e. $\beta = 2$, while it is only first order in case of larger diffusion velocities, i.e. $\beta = 1$. It is worth to point out that the latter case corresponds to larger diffusion speed, but anyway one order of magnitude smaller than flow speed ($W/U = \epsilon$). In both cases, i.e. $\beta = 2$ and $\beta = 1$, the fluid dynamic equations are fully decoupled from any diffusion dynamics because the total mixture pressure is not defined by any thermodynamic relation but by the incompressible condition.

Some numerical tests were performed for proving the effectiveness of the proposed scheme.

28

In particular, (1) the solvent and dilute test cases were considered first, because they are limiting cases in which the Maxwell–Stefan model reduces to the Fick model. In particular, in the dilute test case, it is possible to derive an effective resistance, which depends on the local molar concentrations, and this makes the test particularly meaningful. The key point is not solving these tests (which has already been done by a lot of LBM schemes) but to solve both tests with the same model and the same set of parameters. In the previous schemes, a special tuning was required to switch between solvent and dilute test case, in order to adapt the diffusion coefficients to the theoretical values. This is not the case for the proposed scheme, because it automatically reproduces the correct transport coefficients, without any special efforts by the user. Moreover (2) some test cases based on the Stefan diffusion tube were performed for proving the complete capabilities of the proposed scheme in solving truly Maxwell–Stefan diffusion problems.

APPENDIX A: COMMENTS ON CHAPMAN-ENSKOG EXPANSION OF KINETIC MODELS DESCRIBING DIFFUSION PROCESSES

In case the single-species momentum is not conserved, as it happens in kinetic models describing diffusion processes, the application of the Chapman-Enskog expansion may lead to ambiguities in some diffusion regimes. Let us consider a proper fluid dynamic scaling for the considered model, namely

$$\epsilon^{\alpha}\frac{\partial f_{\sigma}}{\partial t} + \epsilon V_i \frac{\partial f_{\sigma}}{\partial x_i} = \mathbb{C}_{\sigma} \doteq \lambda \left[\hat{\rho}_{\sigma} \, \mathcal{M} \left(\hat{u}^*_{\sigma i} \right) - f_{\sigma} \right], \tag{A1}$$

where $\alpha \geq 1$ must be specified according to the fluid dynamic regime under consideration: for example, $\alpha = 1$ in case of advective (hyperbolic) scaling, as considered in Ref. [32], or $\alpha = 2$ in case of diffusive (parabolic) scaling, as in Eq. (20). In both cases, the local equilibrium is found in the limiting case of vanishing ϵ (Knudsen number) as the zero of the

collisional operator $\mathbb{C}_\sigma$. According to the discussion reported at the end of Section II A 1, the zero of the collisional operator $\mathbb{C}_\sigma$ is given (for the generic species σ) by

$$f_\sigma^0 = \hat{\rho}_\sigma \, \mathcal{M}\left(\hat{u}_i\right), \tag{A2}$$

where $\hat{u}_i$ is the generic component of the barycentric velocity. Deviations from the previous equilibrium may be due to different effects (e.g. diffusion phenomena and viscous phenomena, in the present paper). Taking into account the original model, since the deviations are due to spatial gradients, the Chapman-Enskog procedure assumes an expansion around the zero of the collision integral, namely

$$f_\sigma = \hat{\rho}_\sigma \, \mathcal{M}\left(\hat{u}_i\right) + O(\epsilon). \tag{A3}$$

The next step is to substitute Eq. (A3) into Eq. (A1) and in particular into the definition of $\hat{u}_{\sigma i}^*(f_\sigma)$, which depends on all species velocities $\hat{u}_{\varsigma i}$, which are combinations of the moments of f_ς, namely

$$\hat{u}_{\sigma i}^*(f_\sigma) = \hat{u}_i + O(\epsilon), \tag{A4}$$

and consequently

$$\mathcal{M}\left(\hat{u}_{\sigma i}^*\right) = \mathcal{M}\left(\hat{u}_i\right) + O(\epsilon). \tag{A5}$$

From the previous expression is clear that, in non-equilibrium case, $\mathcal{M}\left(\hat{u}_{\sigma i}^*\right) \neq \mathcal{M}\left(\hat{u}_i\right)$ because of the diffusion phenomena. Hence substituting Eq. (A3) into Eq. (A1) yields

$$f_\sigma = \hat{\rho}_\sigma \, \mathcal{M}\left(\hat{u}_{\sigma i}^*\right) - \frac{1}{\lambda}\left[\epsilon^\alpha \frac{\partial\left(\hat{\rho}_\sigma \, \mathcal{M}\left(\hat{u}_i\right)\right)}{\partial t} + \epsilon V_i \frac{\partial\left(\hat{\rho}_\sigma \, \mathcal{M}\left(\hat{u}_i\right)\right)}{\partial x_i}\right] + O(\epsilon^2), \tag{A6}$$

which is substantially identical to Eq. (4.17) of Ref. [32]. It is worth to point out that the first Maxwellian $\mathcal{M}$ is centered on $\hat{u}_{\sigma i}^*$ while the second on $\hat{u}_i$. Analyzing the single species momentum equation (see for example, Eq. (5.2) of Ref. [32]), it is possible to estimate the ratio between the characteristic diffusion speed W and the characteristic flow speed U, namely

$$W/U = \mathrm{Kn}\,\mathrm{Ma} = O(\epsilon^\alpha). \tag{A7}$$

Hence the diffusion speed must be smaller than the flow speed (because $\alpha \geq 1$). Taking into account the previous scaling and the property given by Eq. (7) yields $\hat{u}_{\sigma i}^* - \hat{u}_i = O(\epsilon^{2\alpha-1})$ and consequently

$$\mathcal{M}\left(\hat{u}_i\right) = \mathcal{M}\left(\hat{u}_{\sigma i}^*\right) + O(\epsilon^{2\alpha-1}). \tag{A8}$$

30

The previous expression is more precise than Eq. (A5) (because $\alpha \geq 1$). Substituting the previous approximation into Eq. (A6) and taking into account that $2 \leq 2\alpha \leq 3\alpha - 1$ yields

$$f_\sigma = \hat{\rho}_\sigma \, \mathcal{M}\left(\hat{u}_{\sigma i}^*\right) - \frac{1}{\lambda}\left[\epsilon^\alpha \frac{\partial\left(\hat{\rho}_\sigma \, \mathcal{M}\left(\hat{u}_{\sigma i}^*\right)\right)}{\partial t} + \epsilon V_i \frac{\partial\left(\hat{\rho}_\sigma \, \mathcal{M}\left(\hat{u}_{\sigma i}^*\right)\right)}{\partial x_i}\right] + O(\epsilon^2), \qquad (A9)$$

where only the velocity $\hat{u}_{\sigma i}^*$, dictated by the diffusion phenomena and hence by the partial pressure gradients, is involved. Clearly Eq. (A6) and Eq. (A9) represent two different legitimate approximations of f_σ, with the same order of accuracy with regards to ϵ. Let us suppose to take the moments of expression (A6) or (A9), while searching for the macroscopic equations in the continuum limit. Apparently, it could seem that two different sets of macroscopic equations are obtained, when considering as starting point Eq. (A6) or Eq. (A9) respectively. However, because of the property (A7) these two sets of macroscopic equations would be equivalent.

The ambiguities may rise when considering larger diffusion velocities, such that $W/U \gg O(\epsilon^\alpha)$. In the latter case, different asymptotic techniques may produce different results, essentially in between the limiting cases given by Eq. (A6) and by Eq. (A9). For example, assuming $W/U = O(\epsilon^{\alpha-1})$ yields

$$\mathcal{M}\left(\hat{u}_i\right) = \mathcal{M}\left(\hat{u}_{\sigma i}^*\right) + O(\epsilon^{2\alpha-2}), \qquad (A10)$$

and, in case $\alpha = 1$ (advective scaling), taking into account Eq. (A9) and Eq. (A10) yields

$$f_\sigma = \hat{\rho}_\sigma \, \mathcal{M}\left(\hat{u}_{\sigma i}^*\right) + O(\epsilon) = \hat{\rho}_\sigma \, \mathcal{M}\left(\hat{u}_i\right) + O(1). \qquad (A11)$$

Clearly the previous case is far away from equilibrium, because $f_\sigma - \hat{\rho}_\sigma \, \mathcal{M}\left(\hat{u}_i\right) = O(1)$, which contradicts the expansion given by Eq. (A3). However an expansion around $\hat{\rho}_\sigma \, \mathcal{M}\left(\hat{u}_{\sigma i}^*\right)$ is still possible, by reminding that $\hat{u}_{\sigma i}^*$ is unambiguously defined by the partial pressure gradients.

Another example is given by $\alpha = 2$ (diffusive scaling) and $W/U = O(1)$ ($\beta = 0$ in the main text), which yields $\hat{u}_{\sigma i}^* - \hat{u}_i = O(\epsilon)$ and

$$f_\sigma = \hat{\rho}_\sigma \, \mathcal{M}\left(\hat{u}_{\sigma i}^*\right) + O(\epsilon) = \hat{\rho}_\sigma \, \mathcal{M}\left(\hat{u}_i\right) + O(\epsilon). \qquad (A12)$$

Recalling that the diffusive scaling implies $\hat{u}_{\sigma i}^* = \epsilon \, u_{\sigma i}^*$ and $\hat{u}_i = \epsilon \, u_i$, the previous expression yields

$$f_\sigma - \hat{\rho}_\sigma \, \mathcal{M}\left(0\right) = \epsilon \, \hat{\rho}_\sigma \, \mathcal{M}\left(u_{\sigma i}^*\right) + O(\epsilon) = \epsilon \, \hat{\rho}_\sigma \, \mathcal{M}\left(u_i\right) + O(\epsilon) = O(\epsilon), \qquad (A13)$$

which is useless, because it does not discriminate the leading effects of the diffusion process. In the latter case, a different asymptotic technique is recommended.

[1] G. R. McNamara and G. Zanetti, Phys. Rev. Lett. **61**, 2332 (1988).

[2] F. J. Higuera and J. Jiménez, Europhys. Lett. **9**, 663 (1989).

[3] F. J. Higuera, S. Succi, and R. Benzi, Europhys. Lett. **9**, 345 (1989).

[4] H. Chen, S. Chen, and W. Matthaeus, Phys. Rev. A **45**, R5339 (1992).

[5] Y. Qian, D. d'Humières, and P. Lallemand, Europhys. Lett. **17**, 479 (1992).

[6] X. He and L.-S. Luo, Phys. Rev. E **55**, R6333 (1997).

[7] X. Shan and X. He, Phys. Rev. Lett. **80**, 65 (1998).

[8] R. Benzi, S. Succi, and M. Vergassola, Phys. Rep. **222**, 145 (1992).

[9] S. Chen and G. D. Doolen, Annu. Rev. Fluid Mech. **30**, 329 (1998).

[10] G. D. (Editor), ed., *Lattice Gas Methods for Partial Differential Equations* (Addison-Wesley, New York, 1990).

[11] D. Wolf-Gladrow, *Lattice-Gas Cellular Automata and Lattice Boltzmann Models*, no. 1725 in Lecture Notes in Mathematics (Springer-Verlag, Berlin, 2000), 2nd ed.

[12] S. Succi, *The Lattice Boltzmann Equation for Fluid Dynamics and Beyond* (Oxford University Press, New York, 2001), 2nd ed.

[13] V. Sofonea and R. F. Sekerka, Physica A **299**, 494 (2001).

[14] Z. Guo and T. S. Zhao, Phys. Rev. E **68**, 035302(R) (2003).

[15] X. Shan and H. Chen, Phys. Rev. E **47**, 1815 (1993).

[16] E. G. Flekkoy, Phys. Rev. E **47**, 4247 (1993).

[17] X. Shan and H. Chen, Phys. Rev. E **49**, 2941 (1994).

[18] E. Orlandini, W. R. Osborn, and J. M. Yeomans, Europhys. Lett. **32**, 463 (1995).

[19] W. R. Osborn, E. Orlandini, M. R. Swift, J. M. Yeomans, and J. R. Banavar, Phys. Rev. Lett. **75**, 4031 (1995).

[20] M. R. Swift, E. Orlandini, W. R. Osborn, and J. M. Yeomans, Phys. Rev. E **54**, 5041 (1996).

[21] A. Lamura, G. Gonnella, and J. M. Yeomans, Europhys. Lett. **45**, 314 (1999), europhys. Lett.

[22] L.-S. Luo and S. S. Girimaji, Phys. Rev. E **67**, 036302 (2003).

[23] A. Xu, Europhys. Lett. **69**, 214 (2005).

[24] P. C. Fancin, P. C. Philippi, and L. O. E. dos Santos, Future Gener. Comput. Syst. **20**, 945 (2004).

[25] P. Asinari, Phys. Fluids **17**, 067102 (2005).

[26] P. Asinari, Phys. Rev. E **73**, 056705 (2006).

[27] S. Arcidiacono, I. V. Karlin, J. Mantzaras, and C. E. Frouzakis, Phys. Rev. E **76**, 046703 (2007).

[28] S. Arcidiacono, J. Mantzaras, S. Ansumali, I. V. Karlin, and C. E. Frouzakis, Phys. Rev. E **74(5)**, 056707 (2006).

[29] N. Prasianakis, and I. V. Karlin, Phys. Rev. E **78(1)**, 016704 (2008).

[30] F. Williams, *Combustion Theory* (Benjamin/Cumming, California, 1986).

[31] V. Garzò, A. dos Santos, and J. J. Brey, Phys. Fluids A **1**, 380 (1989).

[32] P. Andries, K. Aoki, and B. Perthame, J. Stat. Phys. **106**, 993 (2002).

[33] P. Asinari Phys. Rev. E **77**, 056706 (2008).

[34] W. S. R.B. Bird and E. Lightfoot, *Transport Phenomena* (John Wiley & Sons, New York, 1960).

[35] M. E. McCracken and J. Abraham, Phys. Rev. E **71**, 046704 (2005).

[36] D. J. Holdych and D. Rovas and J. G. Georgiadis and R. O. Buckius, Int. J. Mod. Phys. C **9**, 1393 (1998).

[37] P. L. Bhatnagar, E. P. Gross, and M. Krook, Phys. Rev. **94**, 511 (1954).

[38] M. Junk, A. Klar, and L.-S. Luo, J. Computat. Phys. **210**, 676 (2005).

[39] Y. Sone, *Kinetic Theory and Fluid Dynamics* (Birkhäuser, Boston, 2002), 2nd ed.

[40] P. Asinari and T. Ohwada, Comput. Math. Appl. **58**, 841-861 (2009).

[41] H. Struchtrup J. Stat. Phys. **125**, 3, 565–587 (1996).

[42] Z. L. Guo and T. S. Zhao, Phys. Rev. E **67**, 066709 (2003).

[43] A. Bardow, I. Karlin, and A. Gusev, Europhys. Lett. **75**, 434 (2006).

[44] R. Taylor and R. Krishna, *Multicomponent Mass Transfer* (John Wiley & Sons, New York, 1993).

[45] R. R. J. Heywood and S. Turek, Int. J. Numer. Meth. Fluids **22**, 325 (1996).

[46] M. Junk and Z. Yang (2008), submitted to Comput. Math. Appl.

[47] W. V. W.H. Press, S.A. Teukolsky and B. Flannery, *Numerical Recipes 3rd Edition: The Art of Scientific Computing* (Cambridge University Press, Hong Kong, 2007).

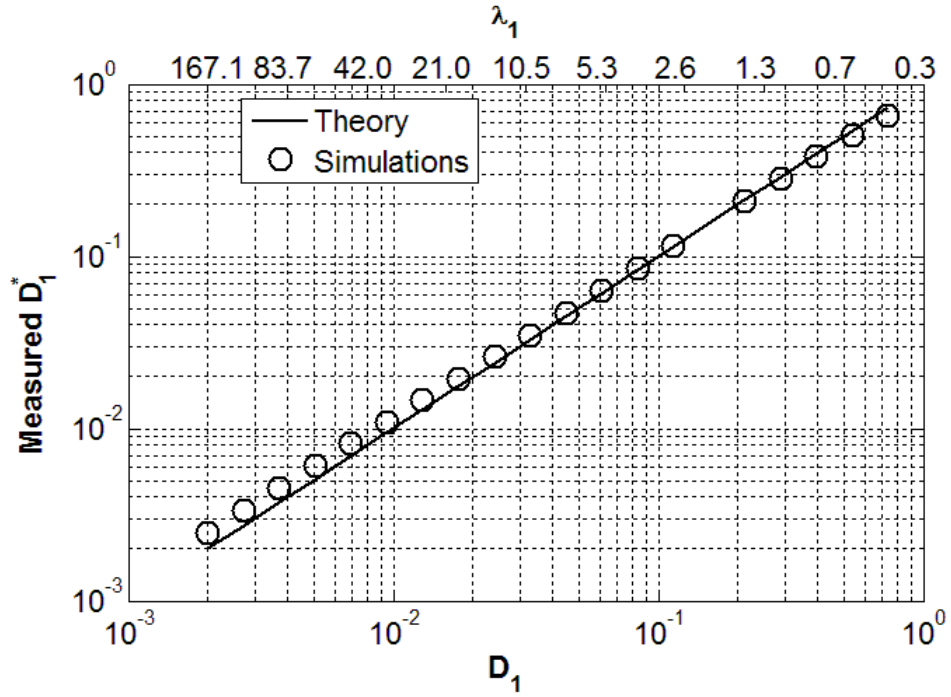[48] R. Krishna and J. Wesselingh, Chemical Engineering Science **52**, 861 (1997).

FIG. 1: Solvent test case for a ternary mixture: $y_3 \approx 1$ and consequently $y_1 \approx 0$ and $y_2 \approx 0$. Comparison between expected Fick diffusion coefficient for component 1, i.e. D_1, with the transport coefficient D_1^* from the numerical implementation of the generalized Fick model, measured by Eq. (91) at time $T = 30\,\delta t$ and spatial location $x = L/2$. The corresponding values for the relaxation frequencies λ_1 are reported as well (dimensionless units).
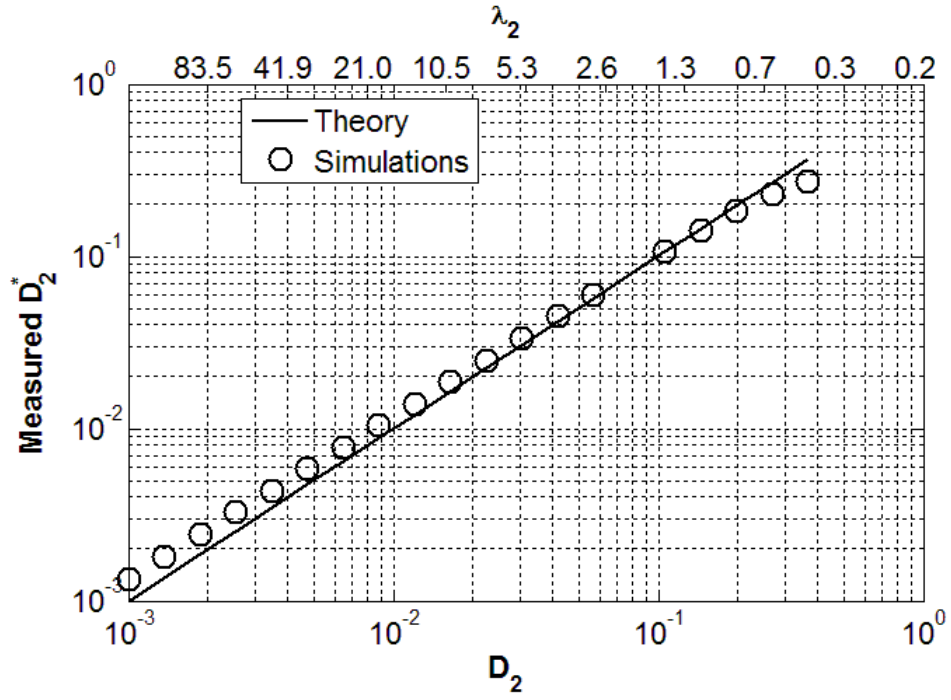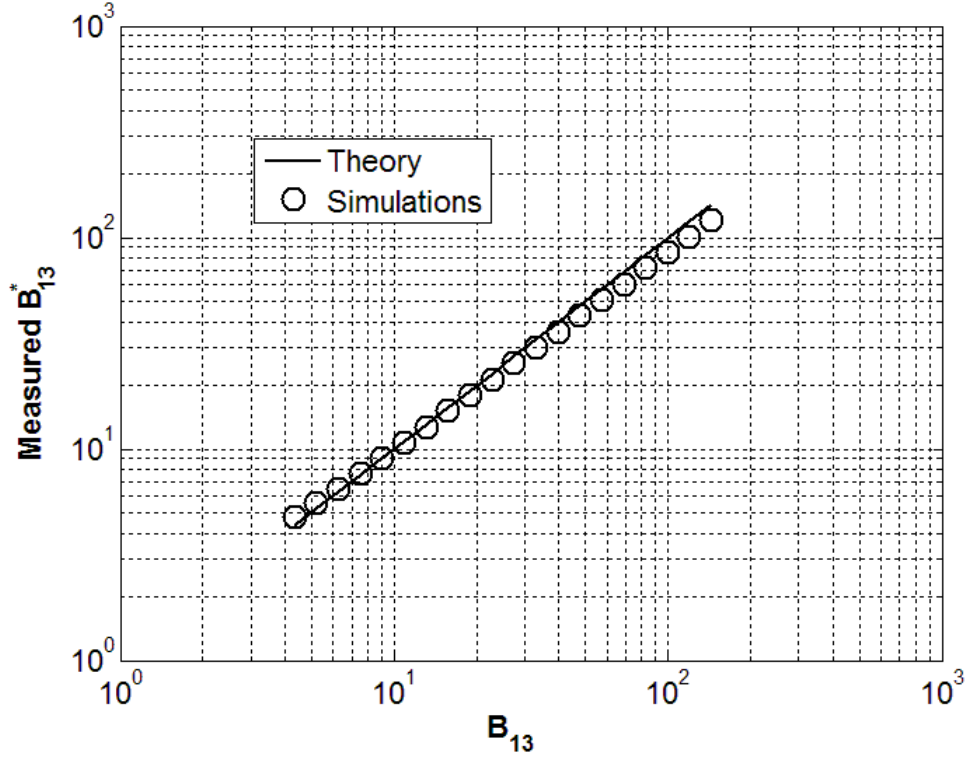
FIG. 2: Solvent test case for a ternary mixture: $y_3 \approx 1$ and consequently $y_1 \approx 0$ and $y_2 \approx 0$. Comparison between expected Fick diffusion coefficient for component 2, i.e. D_2, with the transport coefficient D_2^* from the numerical implementation of the generalized Fick model, measured by Eq. (92) at time $T = 30\,\delta t$ and spatial location $x = L/2$. The corresponding values for the relaxation frequencies λ_2 are reported as well (dimensionless units).

FIG. 3: Solvent test case for a ternary mixture: $y_3 \approx 1$ and consequently $y_1 \approx 0$ and $y_2 \approx 0$. Comparison between expected Maxwell–Stefan resistance coefficient for component 1, i.e. B_{13}, with the resistance coefficient B_{13}^* from the numerical implementation of the Maxwell–Stefan model, measured by Eq. (91) (dimensionless units).
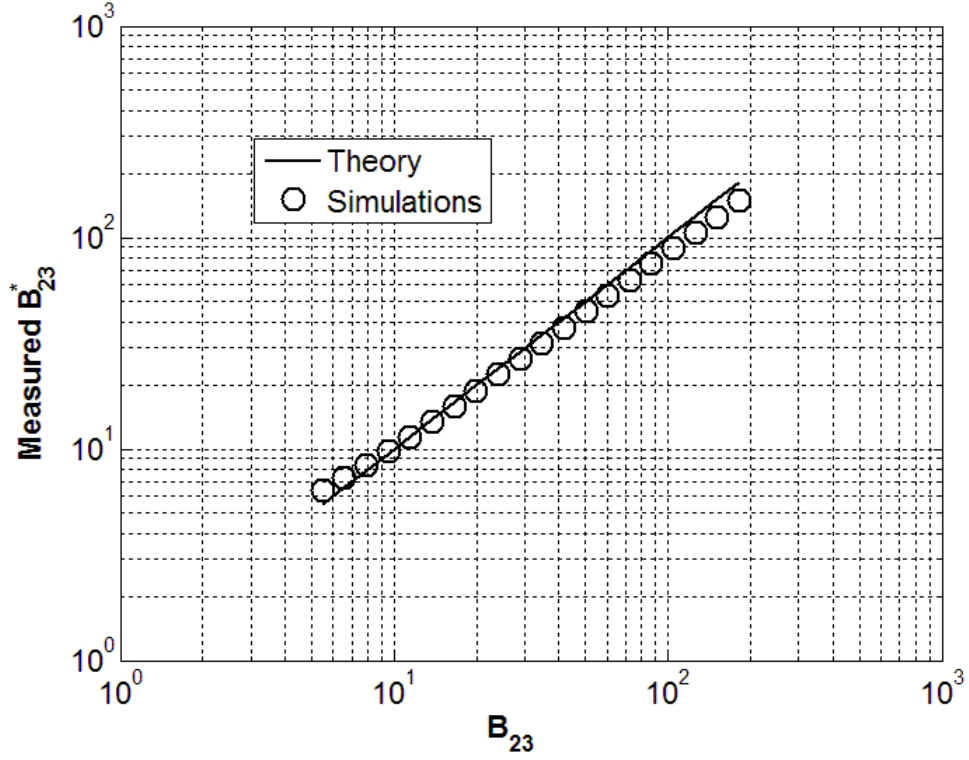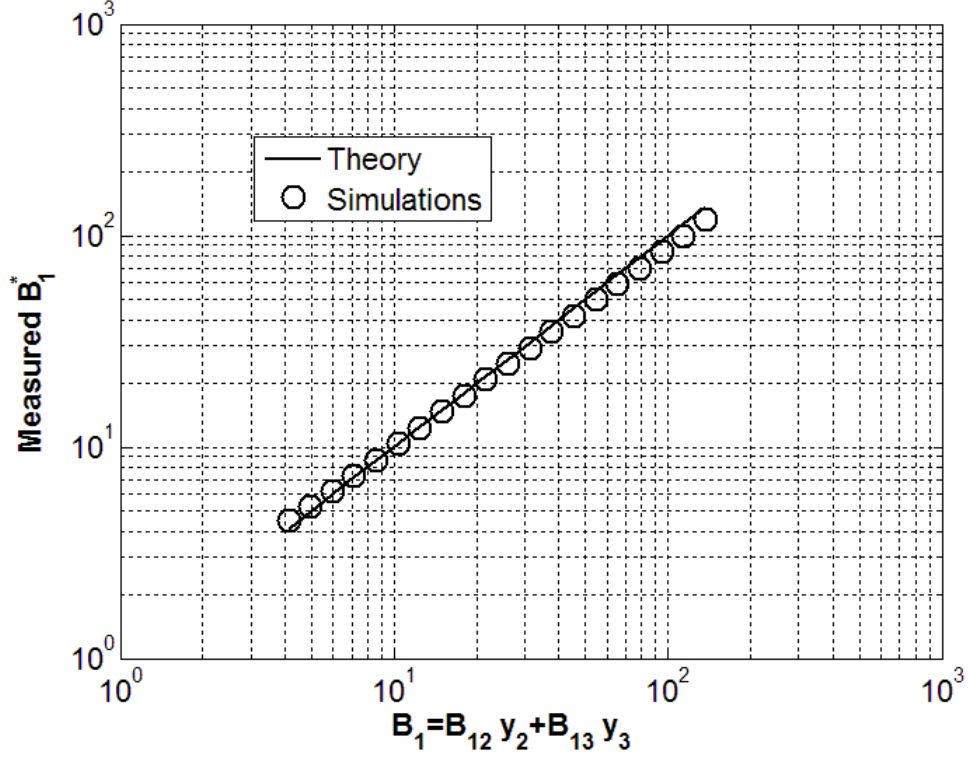
FIG. 4: Solvent test case for a ternary mixture: $y_3 \approx 1$ and consequently $y_1 \approx 0$ and $y_2 \approx 0$. Comparison between expected Maxwell–Stefan resistance coefficient for component 2, i.e. B_{23}, with the resistance coefficient B_{23}^* from the numerical implementation of the Maxwell–Stefan model, measured by Eq. (92) (dimensionless units).

FIG. 5: Dilute test case for a ternary mixture: $y_1 \approx 0$ and consequently $y_1 \ll y_2 + y_3$. Comparison between expected Maxwell–Stefan equivalent effective resistance for component 1, i.e. B_1, with the resistance coefficient B_1^* from the numerical implementation of the Maxwell–Stefan model, measured by Eq. (97) (dimensionless units).
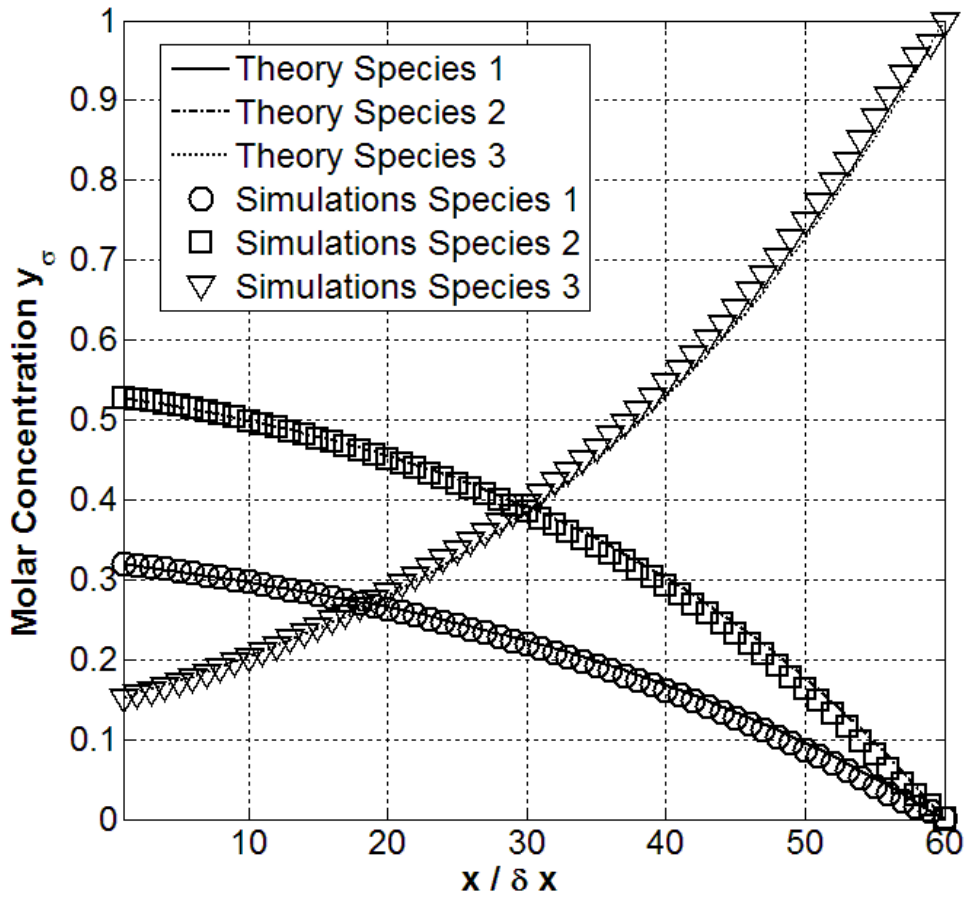
FIG. 6: Non-Fickian test case: composition profiles in a Stefan diffusion tube. Zero flux is assumed for the gas carrier, i.e. $N_3 = 0$. The reference solutions are obtained by solving the boundary value problem by the shooting method and a multi-variable Newton method (dimensionless units).
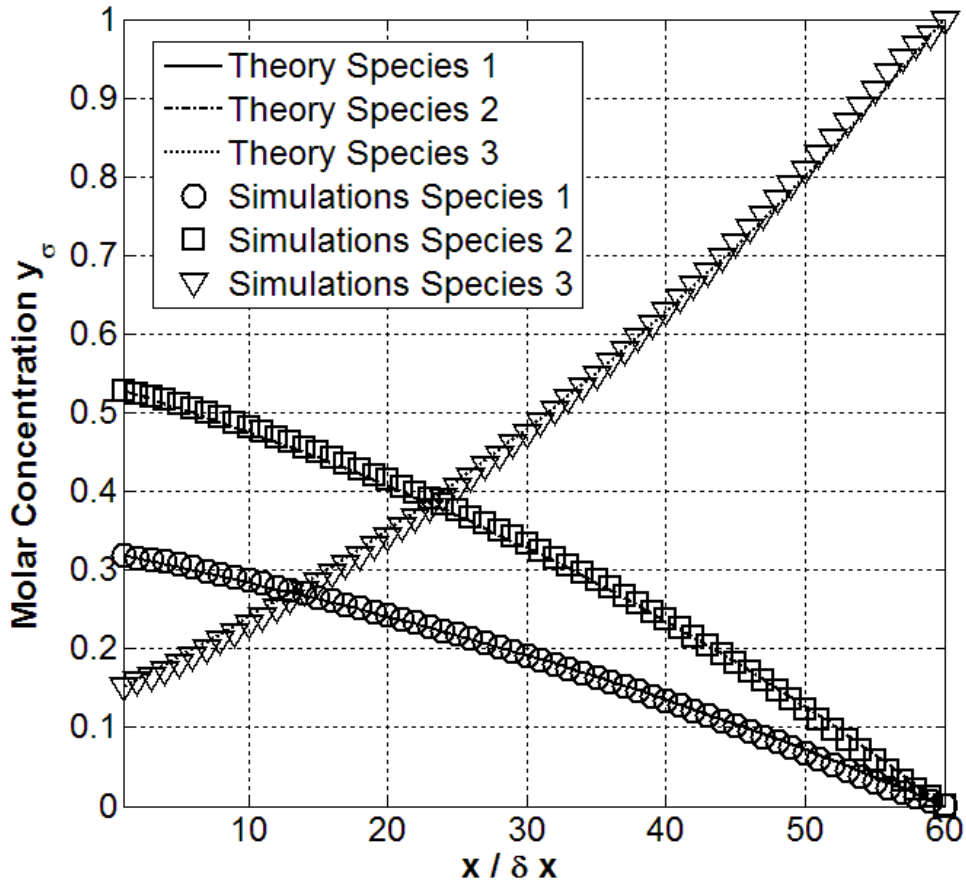
FIG. 7: Non-Fickian test case: composition profiles in a Stefan diffusion tube. Negative flux is assumed for the gas carrier pointing toward the liquid bottom ($x = 0$), i.e. $N_3 = -6.1776 \cdot 10^{-5}$. The reference solutions are obtained by solving the boundary value problem by the shooting method and a multi-variable Newton method (dimensionless units).